Free Oscillations: Frequencies and Attenuations

T. G. Masters and R. Widmer

1. INTRODUCTION

The displacement at any point on the surface of the Earth can be quite complicated but can be thought of as a sum of discrete modes of oscillation, each mode having a characteristic frequency and decay rate which are dependent upon the structure of the Earth. The initial amplitudes of the modes of free oscillation depend upon the source of excitation which, in free-oscillation seismology (or "normal mode" seismology), is usually an earthquake. Earthquakes are typically of relatively short duration. For example, a magnitude 6.5 earthquake will rupture for perhaps ten seconds after which the Earth is in free oscillation. Away from the immediate vicinity of the earthquake, the motions of the Earth are small in amplitude and the total displacement at a recording site can be written simply as a sum of decaying cosinusoids:

$$u(t) = \sum_k A_k \cos{(\omega_k t + \phi_k)} e^{-\alpha_k t}. \tag{1}$$

ω_k is the frequency of the k'th mode which has an initial amplitude A_k and an initial phase ϕ_k. α_k controls the decay rate of the k'th mode and is often written in terms of the "quality" of the mode, Q_k, where

$$Q_k = \frac{\omega_k}{2\alpha_k}. \tag{2}$$

T. G. Masters and P. M. Shearer, University of California, San Diego, IGPP, A025, La Jolla, CA 92093

104

When Q_k is large, α_k is small so the mode rings on for a long time. Conversely, low Q modes decay away quickly. In the Earth, attenuation of seismic energy is weak and the Q's of modes are typically between 100 and 6000. Thus modes of oscillation ring on for many cycles before being appreciably attenuated.

Long wavelengths are typically associated with low frequencies and free oscillation theory has usually been used to describe motions of the Earth with periods between about 100 seconds and 1 hour. The latter period corresponds to the frequency of the mode $_0S_2$ which is sometimes called the "football mode" of the Earth since it corresponds to a mode of deformation in which the Earth looks like an American football (Figure 1a). The notation $_nS_\ell$ arises from the fact that, on a spherically-symmetric Earth, free oscillations have displacement fields which are simply related to spherical harmonics: the ℓ is the harmonic degree of the relevant spherical harmonic which controls the number of nodes in the displacement field in latitude. n is the "overtone index". $n = 0$ corresponds to the lowest frequency mode of harmonic degree ℓ and is termed a "fundamental mode". Higher frequency modes, $n > 0$, are called "overtones". Finally, the S indicates that this mode is in the class of "spheroidal" modes. Spheroidal modes can have complicated displacement fields which involve compression of the Earth as well as shearing. These modes therefore affect (and are affected by) the gravitational field of the Earth and can be measured using gravimeters. The simplest case of a spheroidal mode is one in which the displacement is everywhere in the radial direction (Figure 1b). Such modes are called "radial" modes and the fundamental radial mode, $_0S_0$, has a period of about 20 minutes. An alternate class of modes is the "toroidal modes" which consist of shearing on concentric shells (e.g., Figure 1c) and are labelled $_nT_\ell$ in an analogous fashion to the
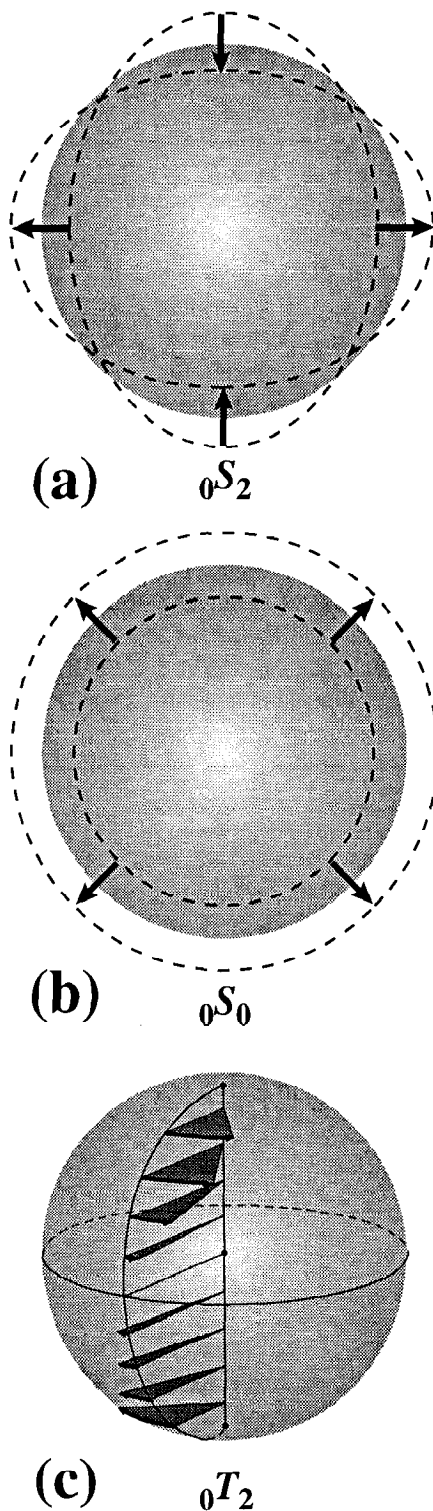
Fig. 1. Illustrations of the displacement fields of various modes of oscillation. a) $_0S_2$, the "football" mode of the Earth, b) $_0S_0$, the "breathing" mode of the Earth, and c) the toroidal mode $_0T_2$.
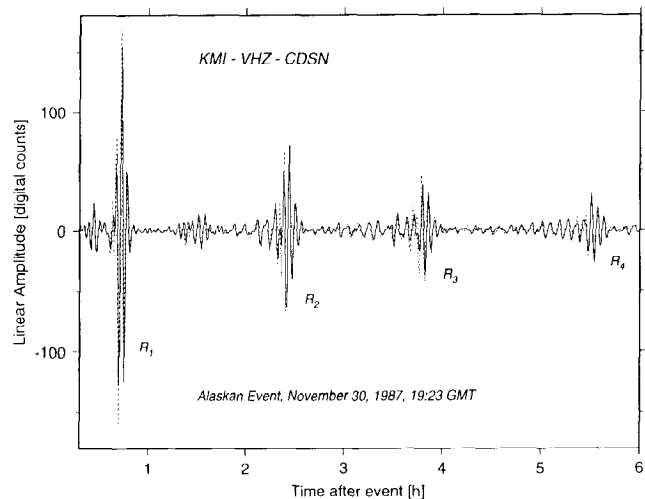

Fig. 2. Comparison of a synthetic seismogram with data for a vertical-component, long-period recording (VHZ) from a station of the Chinese Digital Seismic Network at Kunming (KMI). The dotted line is the synthetic made by mode summation and includes all modes with frequencies less then 8 mHz. The large wave packets labelled R_1–R_4 are Rayleigh wave surface waves. R_1 has travelled the minor arc from the source to receiver while R_2 has travelled in the opposite direction. The travel time to complete a full orbit is about 3 hours (R_3 is the same as R_1 but after one complete orbit).

spheroidal modes. The motion in a toroidal mode has no radial component and there is no compression or dilation so they are not recorded on gravimeters.

Low frequency disturbances are efficiently excited only by large earthquakes so the study of free oscillations has historically concerned the study of very large earthquakes. Modern networks can easily record free oscillations from earthquakes with surface wave magnitudes greater than about 6.5. There are roughly 20 such events per year so there are now many thousands of recordings available for free-oscillation research. An example of a long-period recording is shown in Figure 2 along with a "synthetic" seismogram made using equation (1). A model of the earthquake source is used to calculate the initial amplitude and phase (A_k and ϕ_k) of each mode and a model of the elastic and anelastic properties of the Earth is used to calculate the frequency and attenuation rate (ω_k and α_k) of each mode. Even though equation (1) is very simple, the interference between modes of oscillation gives a complicated waveform which agrees in detail with the observations. The large amplitude wave packets seen in the seismogram correspond to surface waves which travel around the surface of the Earth much like ripples on the

surface of a pond travelling away from some initial disturbance.

It is interesting to note that the particular Earth model used in this calculation is rather simple. In fact the model includes only radial variations of the elastic and anelastic parameters and completely ignores lateral variations such as continent/ocean differences. Such spherically-symmetric Earth models can quite accurately reproduce many seismic observations and provide useful starting approximations to more realistic calculations.

Much of the theory used to calculate the free oscillations of Earth models has been available for over a century but the observational history is much shorter. The initial "observation" was made by Benioff [3] who recorded a long-period disturbance of the Earth on a fused-quartz strainmeter after a large earthquake in Kamchatka in 1952. Benioff's interpretation of this record is almost certainly wrong but this work did reawake interest in the theoretical aspects of free-oscillations [e.g., 1]. Thus, in 1960, code for computing the free-oscillation frequencies of realistic Earth models existed just as the huge Chilean earthquake provided the first unambiguous recordings. Several groups presented observations of spheroidal modes measured on gravimeters and spheroidal and toroidal modes measured on strainmeters and the good agreement with the calculated frequencies gave strong support to the results (particularly convincing was the lack of peaks at the computed toroidal mode frequencies on the gravimeter recordings). Recordings from this event also provided the first observational evidence for splitting of the lowest frequency modes caused by the rotation of the Earth [2, 25].

The occurrence of several huge earthquakes throughout the 60's and the installation of the WWSSN (Worldwide Standardized Seismographic Network) in the early 60's resulted in many further observations of mode frequencies which are summarized in Derr [9] and were used in several attempts to make better Earth models.

The next major step forward came with the occurrence of the Columbian 1970 earthquake. This remarkable earthquake was as large as anything recorded digitally since but was at a depth of 650 km. Such deep earthquakes are incapable of exciting fundamental modes which normally dominate the seismogram and obscure the lower amplitude overtones. Consequently, the Colombian earthquake allowed a great number of overtones to be measured for the first time. These modes are important since they constrain the structure of the deep Earth. A gravimeter recording of this event was made at Payson Arizona by W. Farrell and the spectrum (see next section) is completely dominated by overtones, some of which have not been reliably observed since! It is this recording which provided

the impetus to start the global IDA (International Deployment of Accelerometers) array in the mid-70's. Theoretical work by Gilbert in the early 70's also led to compact expressions for mode excitation and array processing algorithms which were eventually applied to hand-digitized WWSSN recordings of the Columbian earthquake [16]. The resulting explosion in the number and quality of degenerate frequency estimates led to a dataset which is essentially that used in the construction of current reference Earth models [e.g., 11]. Subsequent work using data from the modern digital arrays has led to the identification of large signals due to Earth rotation and 3-dimensional structure which must be assessed before accurate degenerate frequencies can be assigned.

2. FREE-OSCILLATION FREQUENCIES AND ATTENUATION RATES

The utility of the free-oscillation description of long-period seismic motion becomes apparent when we look at the spectrum of a seismic recording. Figure 3 shows the amplitude spectrum of 60 hours of the recording of Figure 2. The spectrum is clearly composed of discrete peaks, each peak corresponding to one (or more) mode of free
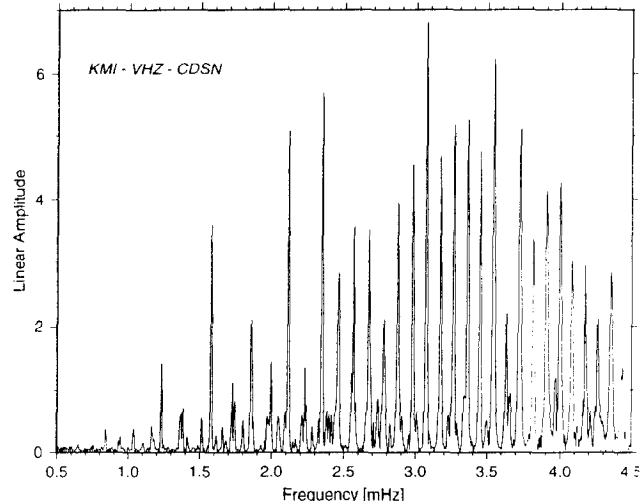
Fig. 3. Fourier amplitude spectrum of 60 hours of the recording shown in Figure 2. The record was Hanning-tapered to reduce spectral leakage effects. The spectrum (which is proportional to ground acceleration) is dominated by large peaks which are roughly uniformly spaced with a separation of about 0.1 mHz. These peaks correspond to fundamental spheroidal modes which compose the large amplitude Rayleigh wave packets seen in Figure 2.

oscillation. If a peak can be identified as a particular mode of oscillation and the peak frequency accurately measured, we can use the frequencies to improve our models of the Earth. The width of each spectral peak is also related to the attenuation of a mode – slowly attenuating modes have narrow spectral peaks while strongly attenuated modes have broad spectral peaks. We can, in principle, measure the attenuation rate of each mode and thus learn about the attenuation characteristics of the Earth.

The situation is much more complicated in practice due to the small departures from spherical symmetry in the real Earth. To understand this, we require some theory (the details are relegated to the Appendix). We find that, on a spherically symmetric Earth, there are two classes of oscillation: spheroidal and toroidal (see equations 15,16). The displacement fields are proportional to a spherical harmonic of degree ℓ or its lateral derivatives though the frequencies of free oscillation are independent of the azimuthal order number m. A consequence of this is that there are $2\ell + 1$ modes of oscillation with exactly the same frequency. This group of $2\ell + 1$ modes is called a "multiplet" while the individual members of the multiplet are called "singlets". Departures of the Earth from spherical symmetry remove the degeneracy and, in general, each singlet within a multiplet will have a slightly different frequency. This phenomonon is called "splitting".

Figure 4 shows the degenerate frequencies of toroidal and spheroidal oscillation for a typical spherically symmetric Earth model, PREM, for frequencies below 10 mHz. The large dots indicate those degenerate frequencies which can be reliably determined (see also Table 1). There is considerable structure in these diagrams and modes are often classified into various types to help describe their properties. Consider the simpler case of toroidal modes. Once the displacement field is known for a mode, it is straightforward to calculate the distribution of energy of the mode within the Earth (see Appendix). Figure 5 shows the elastic shear energy density for three different toroidal modes as a function of radius. The first is a fundamantal mode ($n = 0$) and the energy is confined close to the surface. If we use equation (1) to calculate a synthetic seismogram and include only fundamental modes, we generate a seismogram consisting of the large amplitude surface waves (actually Love waves). Fundamental modes are therefore called "surface-wave equivalent" modes. The second example is of a mode whose energy distribution is oscillatory part way through the mantle then becomes exponentially decaying. The depth at which the behavior changes from oscillatory to exponential is called the "turning point". If a seismogram is constructed of all modes with a turning point at this depth, we find that it looks like
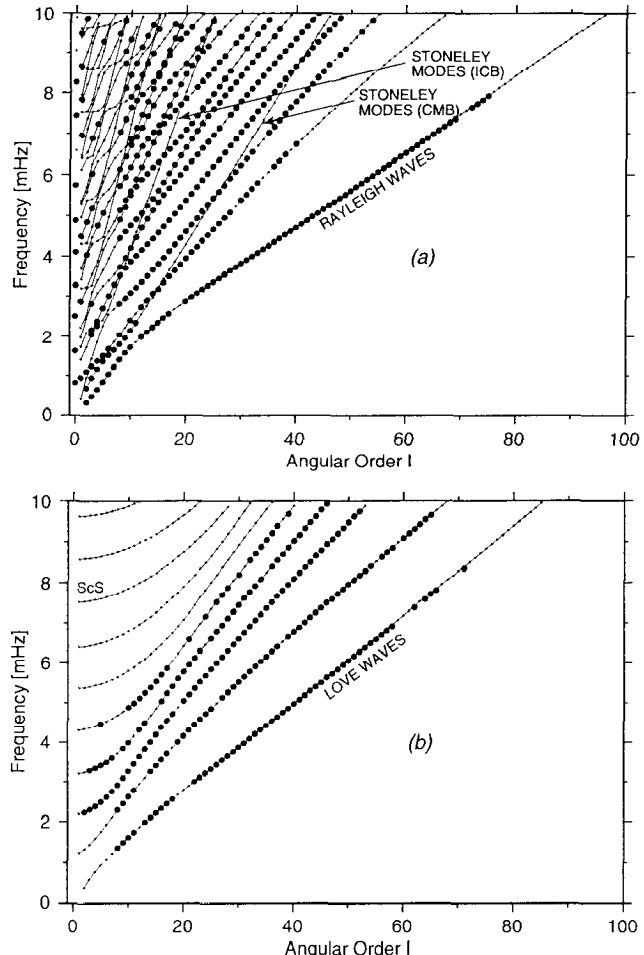
Fig. 4. Free-oscillation frequencies (dots) plotted as a function of harmonic degree for a) spheroidal modes and b) toroidal modes. The large dots indicate the modes for which a reliable degenerate frequency can be assigned (see Table 1). The solid lines join modes of the same overtone number and are called "branches". The fundamental mode branch is the lowest frequency branch and is equivalent to the dispersion curve for fundamental mode surface waves. Also marked in figure 4a are the pseudobranches corresponding to waves trapped on the CMB and on the ICB (a pseudobranch is made up of several segments of different overtone branches). The very steep pseudobranches in the top left of figure 4a are composed of modes which have their energy trapped inside the inner core while the nearly flat pseudobranches which cross them are composed of ScS-equivalent and PcP-equivalent modes.

a set of body wave S arrivals (e.g. S, SS, SSS, etc.) all of which have the same ray turning point. Such modes are called "mantle S-equivalent" modes. The final example is oscillatory all the way through the mantle. In fact, all

TABLE 1. Mode frequencies and attenuations

Mode	f_{obs} μHz	f_{PREM} μHz	q_{obs}^a	q_{PREM}	ref.[b]	Mode	f_{obs} μHz	f_{PREM} μHz	q_{obs}	q_{PREM}	ref.
$_0S_2$	309.45 ± 0.15	309.28	1.23 ± .30	1.962	26[c]	$_0T_{15}$	2212.15 ± 0.40	2210.34	5.96 ± .25	6.572	32[c]
$_0T_2$	377.30 ± 0.80	379.17		3.994	37[c]	$_7S_1$		2224.25		4.018	
$_2S_1$		403.96		2.520		$_2S_9$		2228.75		5.312	
$_0S_3$	468.55 ± 0.15	468.56	2.63 ± .31	2.395	26[c]	$_2T_2$		2230.84		4.878	
$_0T_3$	587.60 ± 0.70	586.16		4.167	37[c]	$_0S_{14}$	2229.60 ± 0.25	2231.40	3.02 ± .10	3.352	32[c]
$_0S_4$	646.80 ± 0.20	647.07	2.74 ± .22	2.680	27[c]	$_3S_5$		2234.54		11.122	I
$_1S_2$	680.00 ± 0.30	679.85	2.71 ± .51	3.222	26[c]	$_4S_4$	2279.65 ± 0.45	2279.60		3.446	26
$_0T_4$	766.90 ± 0.40	765.66		4.382	37[c]	$_1T_8$	2281.00 ± 2.50	2280.23		4.308	34
$_0S_0$	814.39 ± 0.01	814.31	0.17 ± .01	0.188	21[c]	$_2T_3$		2294.97		4.836	
$_0S_5$	840.08 ± 0.10	840.42	2.86 ± .10	2.812	27	$_0T_{16}$	2327.03 ± 0.40	2325.19	6.08 ± .23	6.690	32[c]
$_0T_5$	928.55 ± 0.25	928.24	3.89 ± .25	4.621	37[c]	$_0S_{15}$	2344.75 ± 0.20	2346.38	2.92 ± .08	3.463	32[c]
$_2S_2$		937.85		10.432	I	$_1S_{11}$	2346.50 ± 1.00	2347.54		2.674	34
$_1S_3$	939.60 ± 0.25	939.83	3.01 ± .14	3.537	27	$_5S_4$	2379.17 ± 0.20	2379.52	2.11 ± .12	2.044	27
$_3S_1$	944.20 ± 0.30	943.95	1.25 ± .12	1.209	34[c]	$_2T_4$		2379.86		4.775	
$_0S_6$	1037.55 ± 0.10	1038.21	2.91 ± .13	2.879	27[c]	$_2S_{10}$	2404.00 ± 0.70	2402.93	4.51 ± .10	5.518	32
$_0T_6$	1078.90 ± 0.20	1078.83	4.01 ± .37	4.868	37[c]	$_6S_2$		2410.68		10.788	I
$_3S_2$	1106.00 ± 0.40	1106.21	2.66 ± .29	2.728	27[c]	$_4S_5$		2411.43		3.541	
$_1S_4$	1172.77 ± 0.10	1172.85	3.76 ± .18	3.689	27	$_0T_{17}$	2441.35 ± 0.50	2439.09	5.42 ± .23	6.795	32[c]
$_0T_7$	1221.50 ± 0.40	1220.70	4.65 ± .52	5.112	37	$_1T_9$	2452.00 ± 1.00	2452.49		4.399	34
$_0S_7$	1230.96 ± 0.20	1231.79	3.21 ± .15	2.923	27	$_0S_{16}$	2456.80 ± 0.15	2458.22	3.08 ± .08	3.586	32[c]
$_1T_1$		1236.11		3.847		$_2T_5$		2485.09		4.693	
$_2S_3$	1242.96 ± 0.10	1242.19	2.53 ± .20	2.407	27	$_2S_0$	2507.90 ± 0.20	2510.48	0.56 ± .14	.805	21
$_1T_2$		1320.13		3.901		$_7S_2$		2517.29		2.929	
$_0T_8$	1356.70 ± 0.30	1356.11	4.95 ± .33	5.346	34	$_3S_6$		2549.64		3.629	
$_1S_5$	1370.01 ± 0.20	1370.27	3.02 ± .27	3.426	27	$_0T_{18}$	2554.40 ± 0.70	2552.22	6.18 ± .29	6.890	32[c]
$_2S_4$	1379.60 ± 0.20	1379.20	2.55 ± .15	2.630	27	$_1S_{12}$		2555.06		2.738	M
$_4S_1$		1412.64		2.817		$_0S_{17}$	2565.35 ± 0.30	2567.12		3.719	32[c]
$_0S_8$	1412.74 ± 0.10	1413.51	2.92 ± .20	2.964	27[c]	$_2S_{11}$		2572.16		5.676	
$_3S_3$		1417.19		11.000	I	$_2T_6$		2610.08		4.591	
$_1T_3$		1439.13		3.955		$_1T_{10}$	2619.00 ± 2.00	2620.02		4.479	34
$_0T_9$	1487.30 ± 0.20	1486.61	5.24 ± .27	5.566	34[c]	$_4S_6$		2626.93		11.136	I
$_2S_5$	1515.27 ± 0.30	1514.93		3.309	27	$_0T_{19}$		2664.71		6.974	
$_1S_6$	1521.36 ± 0.40	1522.04	2.64 ± .35	2.893	27	$_0S_{18}$		2673.30		3.860	
$_0S_9$	1577.37 ± 0.20	1578.28	2.80 ± .12	3.005	27[c]	$_3S_7$		2686.33		3.713	
$_1T_4$		1585.50		4.006		$_5S_5$	2703.67 ± 0.20	2703.36	1.89 ± .15	1.990	27
$_0T_{10}$	1614.10 ± 0.45	1613.26	5.32 ± .29	5.773	34[c]	$_2S_{12}$	2736.60 ± 0.50	2737.31	4.58 ± .10	5.769	32
$_1S_0$	1631.36 ± 0.05	1631.34	0.54 ± .06	0.667	21[c]	$_2T_7$		2753.73		4.476	
$_1S_7$	1654.48 ± 0.20	1655.51	2.31 ± .08	2.687	27	$_1S_{13}$		2766.24		2.895	M
$_2S_6$	1681.17 ± 0.20	1680.84	3.38 ± .16	4.203	27	$_0T_{20}$		2776.67		7.050	
$_5S_1$		1713.79		11.019	I	$_0S_{19}$		2776.98		4.006	
$_4S_2$		1722.30		2.303		$_1T_{11}$	2783.00 ± 1.00	2783.31		4.546	34
$_0S_{10}$	1725.25 ± 0.20	1726.47	2.79 ± .10	3.050	32[c]	$_3S_8$	2819.02 ± 0.30	2819.64	3.33 ± .17	3.794	27
$_0T_{11}$	1738.25 ± 0.45	1736.85	5.06 ± .39	5.963	32[c]	$_6S_3$	2821.87 ± 0.10	2821.72	2.23 ± .16	2.345	27
$_1T_5$		1750.49		4.061		$_8S_1$	2872.85 ± 0.15	2873.36	1.02 ± .16	1.075	26
$_1S_8$	1797.76 ± 0.10	1799.30	2.31 ± .25	2.635	27	$_0S_{20}$	2877.95 ± 0.20	2878.37	3.55 ± .08	4.154	33[c]
$_3S_4$		1833.30		11.113	I	$_0T_{21}$	2886.90 ± 0.70	2888.20	6.37 ± .20	7.118	32[c]
$_0T_{12}$		1857.94		6.138		$_2S_{13}$	2903.50 ± 2.00	2899.90		5.738	34
$_0S_{11}$		1862.42		3.105		$_2T_8$	2913.00 ± 4.50	2913.97		4.363	34
$_2S_7$		1864.96		4.726		$_1T_{12}$		2943.21		4.601	
$_1T_6$	1925.51 ± 0.45	1925.61		4.129	37	$_3S_9$	2951.50 ± 1.50	2951.58		3.865	34
$_1S_9$	1961.72 ± 0.60	1963.74	2.37 ± .25	2.629	27	$_1S_{14}$		2975.79		3.408	M
$_0T_{13}$	1979.15 ± 0.45	1976.99	5.05 ± .27	6.297	32[c]	$_0S_{21}$	2977.05 ± 0.15	2977.73	3.61 ± .06	4.303	33[c]
$_6S_1$		1980.38		1.538		$_0T_{22}$	2998.80 ± 0.70	2999.37	7.05 ± .27	7.178	32[c]
$_0S_{12}$	1988.70 ± 0.30	1990.37	2.84 ± .10	3.173	32[c]	$_5S_6$	3011.54 ± 0.20	3010.69	1.80 ± .08	1.975	27
$_4S_3$	2048.11 ± 0.30	2048.97	1.60 ± .18	2.083	27	$_4S_7$		3013.63		11.151	I
$_2S_8$	2049.44 ± 0.30	2049.21	4.14 ± .10	5.057	27	$_2S_{14}$	3062.00 ± 1.50	3063.60		5.322	34
$_5S_2$		2091.28		3.146		$_0S_{22}$	3074.60 ± 0.15	3075.27	3.87 ± .06	4.450	33[c]
$_0T_{14}$	2096.25 ± 0.40	2094.36	5.55 ± .31	6.442	32[c]	$_7S_3$		3082.21		11.190	I
$_1T_7$		2103.79		4.214		$_3S_{10}$	3081.50 ± 1.00	3084.79		3.933	34
$_0S_{13}$	2111.55 ± 0.15	2112.94	2.84 ± .10	3.255	32[c]	$_2T_9$	3092.00 ± 7.00	3087.52		4.265	34
$_1S_{10}$	2150.00 ± 4.50	2148.42		2.643	34	$_6S_4$		3092.11		2.894	
$_5S_3$	2168.67 ± 0.20	2169.66	2.80 ± .23	3.420	27	$_1T_{13}$		3100.46		4.648	
$_2T_1$		2187.83		4.904		$_0T_{23}$	3109.10 ± 0.70	3110.25	7.19 ± .23	7.232	33[c]

TABLE 1. continued

Mode	f_{obs} μHz	f_{PREM} μHz	q^a_{obs}	q_{PREM}	ref.[b]	Mode	f_{obs} μHz	f_{PREM} μHz	q_{obs}	q_{PREM}	ref.
$_1S_{15}$	3169.00 ± 2.50	3170.55		4.922	34	$_3T_9$	3843.00 ± 5.00	3853.78		4.276	34
$_0S_{23}$	3170.65 ± 0.10	3171.26	3.86 ± .06	4.594	33[c]	$_1T_{18}$		3859.82		4.874	
$_9S_1$		3197.91		4.486		$_4S_{10}$	3864.50 ± 2.00	3864.58		3.307	34
$_3T_1$		3203.50		4.636		$_2S_{18}$		3874.44		2.489	M
$_8S_2$		3214.23		2.954		$_9S_4$		3877.95		1.940	
$_0T_{24}$	3222.00 ± 0.60	3220.90	7.37 ± .26	7.281	32[c]	$_0T_{30}$	3883.00 ± 1.00	3881.75	7.23 ± .29	7.479	38
$_3S_{11}$	3220.60 ± 0.70	3221.27		4.002	34	$_0S_{31}$	3904.85 ± 0.20	3905.40	4.95 ± .08	5.571	33
$_9S_2$		3231.75		2.456		$_1S_{20}$	3944.50 + 2.50	3941.56		6.434	34
$_3T_2$		3234.09		4.615		$_7S_6$		3958.72		1.983	
$_2S_{15}$		3240.89		3.878	M	$_6S_9$	3964.50 ± 2.00	3965.35		3.119	34
$_1T_{14}$	3255.00 ± 1.50	3255.59		4.691	34	$_3S_{16}$	3965.50 ± 1.50	3966.87		4.408	34
$_0S_{24}$	3265.60 ± 0.10	3265.89	3.97 ± .06	4.734	33[c]	$_0T_{31}$	3993.10 ± 1.50	3991.62		7.501	d
$_6S_5$		3266.82		3.683		$_0S_{32}$	3994.05 ± 0.15	3995.04	5.03 ± .10	5.671	33
$_2T_{10}$	3267.50 ± 3.50	3270.21		4.193	34	$_3T_{10}$	3990.00 ± 5.00	3996.61		4.218	34
$_3S_0$	3272.70 ± 0.60	3271.18	0.71 ± .07	.923	21	$_1T_{19}$	4006.00 ± 2.00	4007.17		4.930	34
$_3T_3$		3279.74		4.585		$_4S_{11}$	4009.00 ± 2.00	4010.47		3.513	34
$_8S_3$		3283.64		3.916		$_2T_{14}$	4011.00 ± 4.50	4016.39		4.155	34
$_5S_7$	3291.88 ± 0.30	3290.76	1.91 ± .15	2.029	27	$_{10}S_2$	4042.58 ± 0.20	4032.33	1.17 ± .15	5.217	27
$_0T_{25}$	3332.40 ± 0.50	3331.35	7.26 ± .23	7.324	32[c]	$_{11}S_2$		4058.47		7.638	I
$_1S_{16}$	3341.00 ± 1.00	3338.62		6.024	34	$_0S_{33}$	4082.95 ± 0.20	4084.52	5.24 ± .10	5.766	33
$_3T_4$		3340.20		4.546		$_1S_{21}$	4093.50 ± 2.50	4088.34		6.429	34
$_0S_{25}$	3358.95 ± 0.10	3359.38	4.13 ± .08	4.869	33[c]	$_2S_{19}$		4092.40		2.457	M
$_3S_{12}$	3361.40 ± 0.45	3362.07		4.074	34	$_0T_{32}$		4101.44		7.520	
$_{10}S_1$		3394.09		11.213	I	$_4S_0$	4106.20 ± 0.10	4105.76	0.82 ± .04	1.032	21
$_4S_8$		3396.91		11.160	I	$_3S_{17}$	4124.30 ± 0.90	4125.58		4.497	34
$_6S_6$		3403.86		3.905		$_3T_{11}$		4151.80		4.164	
$_1T_{15}$	3407.00 ± 1.50	3408.95		4.733	34	$_4S_{12}$	4150.00 ± 2.00	4152.98		3.643	34
$_7S_4$		3413.23		2.996		$_1T_{20}$	4152.00 ± 2.50	4153.05		4.990	34
$_3T_5$		3415.15		4.500		$_5S_{10}$		4157.00		11.175	I
$_0T_{26}$	3442.80 ± 0.60	3441.64	7.18 ± .26	7.362	32[c]	$_8S_5$	4165.61 ± 0.20	4166.20	1.63 ± .15	1.636	27
$_2S_{16}$		3443.46		2.821	M	$_0S_{34}$	4172.10 ± 0.25	4173.90	5.06 ± .08	5.857	33
$_0S_{26}$	3451.40 ± 0.10	3451.91	4.29 ± .08	5.000	33[c]	$_2T_{15}$	4190.00 ± 2.00	4196.12		4.180	34
$_2T_{11}$	3456.00 ± 2.50	3457.67		4.150	34	$_6S_{10}$	4211.11 ± 0.30	4210.76		2.822	34
$_1S_{17}$	3495.50 ± 1.00	3493.94		6.309	34	$_0T_{33}$		4211.23	7.52 ± .32	7.537	
$_3T_6$		3504.29		4.449		$_1S_{22}$	4228.50 ± 3.50	4234.40		6.418	34
$_3S_{13}$	3506.20 ± 0.70	3507.44		4.152	34	$_7S_7$		4237.85		2.409	
$_5S_8$	3526.43 ± 0.70	3525.65		2.391	27	$_0S_{35}$	4261.45 ± 0.20	4263.23	5.33 ± .10	5.945	33
$_0S_{27}$	3543.10 ± 0.10	3543.65	4.36 ± .08	5.125	33	$_3S_{18}$	4284.00 ± 1.00	4285.98		4.586	34
$_0T_{27}$		3551.80		7.397		$_4S_{13}$	4294.00 ± 2.00	4295.21		3.728	34
$_6S_7$		3552.60		3.919		$_1T_{21}$	4295.00 ± 1.00	4297.42		5.055	34
$_9S_3$	3557.94 ± 0.50	3554.98	1.30 ± .15	1.286	27	$_{12}S_1$		4300.34		4.466	
$_1T_{16}$	3560.50 ± 1.00	3560.73		4.777	34	$_{10}S_3$		4300.92		3.451	
$_3T_7$		3607.30		4.393		$_4T_1$		4304.57		4.528	
$_0S_{28}$	3634.40 ± 0.10	3634.76	4.61 ± .08	5.244	33	$_2S_{20}$		4310.64		2.440	M
$_1S_{18}$	3642.50 ± 1.50	3644.94		6.395	34	$_3T_{12}$	4317.00 ± 6.00	4318.29		4.120	34
$_2T_{12}$	3640.50 ± 2.50	3646.13		4.134	34	$_0T_{34}$	4322.00 ± 1.50	4321.00	7.52 ± .28	7.553	38
$_3S_{14}$	3655.40 ± 0.60	3657.11		4.234	34	$_9S_5$		4324.87		11.117	I
$_2S_{17}$		3657.42		2.564	M	$_4T_2$		4326.83		4.527	
$_7S_5$		3659.75		2.095		$_{12}S_2$		4330.16		4.357	
$_0T_{28}$	3662.00 ± 0.60	3661.86	7.08 ± .26	7.427	32	$_0S_{36}$	4351.15 ± 0.25	4352.53	5.43 ± .10	6.030	33
$_{11}S_1$		3685.48		1.507		$_4T_3$		4360.07		4.527	
$_8S_4$		3702.73		10.692	I	$_2T_{16}$	4367.00 ± 3.50	4372.15		4.211	34
$_4S_9$	3707.50 ± 1.50	3708.76		2.950	34	$_1S_{23}$	4379.00 ± 2.00	4379.84		6.405	34
$_1T_{17}$	3710.00 ± 1.00	3711.01		4.824	34	$_{10}S_4$		4381.16		4.217	
$_3T_8$		3723.89		4.335		$_4T_4$		4404.14		4.527	
$_0S_{29}$	3724.75 ± 0.15	3725.34	4.50 ± .08	5.358	33	$_0T_{35}$		4430.75	7.11 ± .24	7.566	
$_6S_8$	3737.50 ± 1.00	3737.62		3.615	34	$_8S_6$		4435.24		2.268	
$_0T_{29}$	3772.50 ± 0.70	3771.84	7.39 ± .28	7.455	32	$_4S_{14}$	4433.00 ± 1.50	4439.08		3.784	34
$_5S_9$		3777.80		11.168	I	$_1T_{22}$	4440.00 ± 2.00	4440.27		5.124	34
$_1S_{19}$	3794.00 ± 1.50	3793.89		6.426	34	$_0S_{37}$	4440.70 ± 0.35	4441.84	5.37 ± .10	6.111	33
$_3S_{15}$	3809.80 ± 0.80	3810.48		4.319	34	$_3S_{19}$	4447.00 ± 1.00	4447.56		4.675	34
$_0S_{30}$	3814.85 ± 0.15	3815.52	4.75 ± .08	5.467	33	$_7S_8$	4448.00 ± 1.00	4452.59		3.111	34
$_2T_{13}$	3830.50 ± 3.50	3832.88		4.138	34	$_5S_{11}$	4464.00 ± 2.00	4456.55		2.669	34

TABLE 1. continued

Mode	f_{obs} μHz	f_{PREM} μHz	q_{obs}^a	q_{PREM}	ref.[b]	Mode	f_{obs} μHz	f_{PREM} μHz	q_{obs}	q_{PREM}	ref.
$_4T_5$		4458.81		4.526		$_3T_{16}$	5040.00 ± 4.50	5054.35		4.121	34
$_{11}S_3$		4462.42		2.235		$_0S_{44}$	5069.05 ± 0.65	5069.01	6.03 ± .10	6.615	33
$_{10}S_5$		4469.75		4.129		$_7S_{12}$	5068.50 ± 2.50	5071.02		3.936	34
$_3T_{13}$	4482.00 ± 7.00	4494.38		4.090	34	$_{11}S_5$	5072.64 ± 0.20	5074.41	1.66 ± .10	1.503	27
$_{13}S_1$	4490.00 ± 0.80	4495.73	0.94 ± .07	1.360	34	$_0T_{41}$		5089.15	7.10 ± .30	7.617	
$_4T_6$		4523.86		4.526		$_1S_{28}$	5088.00 ± 5.00	5097.80		6.360	34
$_1S_{24}$	4525.00 ± 3.00	4524.68		6.391	34	$_3S_{23}$	5092.50 ± 2.00	5098.49		4.999	34
$_2S_{21}$		4528.88		2.430	M	$_4T_{12}$	5116.00 ± 6.00	5119.49		4.517	34
$_0S_{38}$	4529.20 ± 0.20	4531.20	5.56 ± .10	6.190	33	$_1T_{27}$	5129.00 ± 2.00	5131.50		5.525	34
$_6S_{11}$		4534.94		11.182	I	$_5S_{14}$	5138.00 ± 2.00	5136.81		2.691	34
$_0T_{36}$	4542.00 ± 2.00	4540.49		7.578	38	$_9S_8$	5138.50 ± 3.50	5144.45		2.117	34
$_2T_{17}$	4543.00 ± 2.00	4544.86		4.245	34	$_0S_{45}$	5157.20 ± 0.40	5159.01	6.01 ± .10	6.680	33
$_1T_{23}$	4580.00 ± 2.00	4581.59		5.198	34	$_2S_{24}$		5182.42		2.447	M
$_4S_{15}$	4583.00 ± 1.50	4585.74		3.820	34	$_{13}S_3$	5194.39 ± 0.10	5193.82	1.28 ± .10	1.101	27
$_4T_7$		4599.04		4.527		$_0T_{42}$	5200.00 ± 2.50	5198.89		7.621	38
$_3S_{20}$	4606.00 ± 1.00	4609.89		4.761	34	$_4S_{19}$	5201.00 ± 2.00	5206.51		3.862	34
$_7S_9$	4612.00 ± 2.50	4617.95		3.548	34	$_2T_{21}$	5202.00 ± 2.50	5210.67		4.399	34
$_0S_{39}$	4618.65 ± 0.20	4620.61	5.58 ± .10	6.266	33	$_8S_9$	5211.00 ± 2.00	5211.87		1.994	34
$_9S_6$		4620.88		3.020		$_6S_{13}$	5233.50 ± 2.50	5233.88		3.944	34
$_0T_{37}$		4650.23	7.53 ± .33	7.588		$_1S_{29}$		5239.29		6.363	
$_8S_7$		4650.46		2.844		$_3T_{17}$	5234.00 ± 8.00	5242.20		4.171	34
$_1S_{25}$	4670.50 ± 3.00	4668.93		6.378	34	$_0S_{46}$	5248.50 ± 0.50	5249.12	6.12 ± .10	6.743	32
$_3T_{14}$		4677.69		4.078		$_4T_{13}$	5243.00 ± 7.00	5251.78		4.505	34
$_{12}S_3$		4683.62		11.585	I	$_3S_{24}$	5262.50 ± 1.50	5261.42		5.050	34
$_4T_8$		4684.10		4.527		$_1T_{28}$	5264.50 ± 2.00	5265.22		5.611	34
$_5S_{12}$	4700.00 ± 0.80	4695.98		2.593	34	$_7S_{13}$		5288.15		11.194	I
$_0S_{40}$	4707.70 ± 0.35	4710.10	5.66 ± .10	6.339	33	$_{12}S_4$		5293.80		11.333	I
$_2T_{18}$	4710.00 ± 2.50	4714.71		4.281	34	$_{15}S_1$		5295.75		1.471	
$_1T_{24}$	4721.00 ± 2.00	4721.36		5.276	34	$_0T_{43}$		5308.63		7.625	
$_4S_{16}$	4730.00 ± 2.50	4735.78		3.842	34	$_5S_{15}$	5328.00 ± 2.00	5330.11		2.894	34
$_2S_{22}$		4746.99		2.424	M	$_0S_{47}$	5338.60 ± 0.50	5339.35	6.10 ± .12	6.804	32
$_0T_{38}$	4762.00 ± 2.00	4759.96	7.02 ± .30	7.597	38	$_{11}S_6$		5351.70		2.158	
$_{11}S_4$	4765.79 ± 0.20	4766.86	1.35 ± .11	1.425	27	$_5T_1$		5353.50		5.012	
$_7S_{10}$	4763.50 ± 4.50	4767.76		3.756	34	$_{16}S_1$		5355.04		4.984	
$_3S_{21}$	4771.00 ± 1.50	4772.64		4.845	34	$_4S_{20}$	5362.00 ± 2.50	5369.24		3.862	34
$_4T_9$		4778.82		4.527		$_5T_2$		5370.60		5.010	
$_0S_{41}$	4798.10 ± 0.30	4799.67	5.88 ± .10	6.411	33	$_2T_{22}$	5366.00 ± 2.50	5372.32		4.440	34
$_1S_{26}$	4812.50 ± 3.00	4812.57		6.368	34	$_{14}S_2$		5374.58		4.938	
$_{13}S_2$	4844.60 ± 0.20	4845.26	1.00 ± .05	1.138	27	$_1S_{30}$	5378.50 ± 4.00	5379.96		6.371	34
$_1T_{25}$	4859.50 ± 2.00	4859.60		5.357	34	$_9S_9$	5378.00 ± 3.50	5389.25		2.696	34
$_3T_{15}$		4865.33		4.089		$_4T_{14}$	5384.50 ± 4.50	5393.54		4.488	34
$_0T_{39}$		4869.69	7.11 ± .30	7.605		$_5T_3$		5396.19		5.007	
$_9S_7$		4872.64		2.041		$_1T_{29}$	5399.50 ± 2.50	5397.51		5.697	34
$_2T_{19}$		4882.09		4.319		$_2S_{25}$		5398.22		2.734	M
$_4T_{10}$	4885.00 ± 5.00	4883.02		4.526	34	$_{14}S_3$		5407.52		4.866	
$_5S_0$	4889.10 ± 0.30	4884.17	0.80 ± .08	1.086	21	$_6S_{14}$	5409.00 ± 2.00	5410.08		3.857	34
$_0S_{42}$	4887.70 ± 0.35	4889.34	5.75 ± .10	6.481	33	$_0T_{44}$		5418.38		7.627	
$_4S_{17}$	4882.50 ± 2.00	4889.38		3.854	34	$_3S_{25}$	5424.50 ± 2.50	5425.56		4.835	34
$_8S_8$	4904.50 ± 2.50	4908.07		2.384	34	$_3T_{18}$	5414.00 ± 7.00	5427.08		4.232	34
$_6S_{12}$		4911.92		11.188	I	$_0S_{48}$	5428.50 ± 0.50	5429.70	6.50 ± .16	6.865	32
$_{10}S_6$		4914.11		11.470	I	$_5T_4$		5430.22		5.002	
$_7S_{11}$	4915.50 ± 3.00	4916.94		3.870	34	$_{13}S_4$		5455.12		4.811	
$_5S_{13}$	4927.50 ± 1.50	4924.40		2.590	34	$_5T_5$		5472.60		4.996	
$_{14}S_1$		4925.38		11.350	I	$_{10}S_7$		5489.22		11.287	I
$_3S_{22}$	4931.50 ± 1.50	4935.56		4.926	34	$_5S_{16}$	5507.00 ± 2.00	5506.96		3.117	34
$_1S_{27}$	4956.00 ± 6.00	4955.54		6.361	34	$_8S_{10}$	5506.00 ± 2.00	5508.75		2.031	34
$_2S_{23}$		4964.89		2.425	M	$_1S_{31}$	5512.50 ± 4.50	5519.76		6.385	34
$_0S_{43}$	4977.35 ± 0.40	4979.12	6.00 ± .12	6.549	33	$_0S_{49}$	5518.70 ± 0.50	5520.16	6.61 ± .15	6.924	32
$_0T_{40}$	4981.00 ± 2.00	4979.42	7.27 ± .30	7.611	d	$_5T_6$		5523.25		4.987	
$_1T_{26}$		4996.30		5.440		$_{12}S_5$		5527.66		4.539	
$_4T_{11}$	4993.50 ± 4.50	4996.59		4.523	34	$_0T_{45}$	5529.00 ± 4.00	5528.13		7.630	38
$_4S_{18}$	5043.00 ± 2.50	5046.41		3.860	34	$_1T_{30}$	5527.50 ± 1.50	5528.40		5.783	34
$_2T_{20}$	5044.50 ± 4.00	5047.32		4.359	34	$_2T_{23}$	5525.50 ± 2.50	5532.41		4.481	34

TABLE 1. continued

Mode	f_{obs} μHz	f_{PREM} μHz	q_{obs}^a	q_{PREM}	ref.[b]	Mode	f_{obs} μHz	f_{PREM} μHz	q_{obs}	q_{PREM}	ref.
$_4S_{21}$	5525.00 ± 2.00	5534.06		3.861	34	$_7S_{15}$		6038.97		11.205	I
$_{14}S_4$	5544.94 ± 0.79	5541.84	1.23 ± .06	1.346	34	$_1T_{34}$	6039.50 ± 3.50	6039.22		6.113	34
$_4T_{15}$	5538.00 ± 7.00	5544.83		4.462	34	$_4T_{18}$		6051.83		4.362	
$_{15}S_2$		5557.32		9.752	I	$_3S_{28}$		6053.73		2.377	M
$_{11}S_7$		5563.67		3.563		$_{11}S_8$		6055.80		11.532	I
$_5T_7$		5582.08		4.976		$_0S_{55}$	6064.80 ± 1.50	6065.26	7.03 ± .14	7.255	34
$_2S_{26}$	5579.00 ± 2.00	5582.65		5.148	34	$_2S_{29}$	6068.50 ± 2.50	6066.18		5.460	34
$_6S_{15}$	5606.50 ± 2.50	5602.51		3.673	34	$_1S_{35}$		6069.14		6.494	
$_3T_{19}$	5607.00 ± 4.50	5608.11		4.296	34	$_0T_{50}$		6076.99		7.630	
$_0S_{50}$	5609.70 ± 0.50	5610.73	6.77 ± .16	6.982	32	$_5T_{13}$		6102.68		4.816	
$_9S_{10}$	5604.50 ± 2.50	5610.93		3.127	34	$_{17}S_1$		6129.05		1.396	
$_3S_{26}$		5620.49		2.489	M	$_3T_{22}$	6120.00 ± 6.00	6129.31		4.456	34
$_0T_{46}$		5637.89		7.631		$_{12}S_8$	6132.42 ± 0.55	6137.17	2.01 ± .11	1.763	34
$_{12}S_6$		5646.58		3.743		$_5S_{20}$	6152.00 ± 3.00	6155.98		3.579	34
$_5T_8$		5649.00		4.961		$_0S_{56}$	6158.90 ± 1.50	6156.48	7.13 ± .15	7.306	34
$_1T_{31}$	5656.00 ± 3.00	5657.96		5.868	34	$_2T_{27}$	6151.00 ± 6.00	6159.71		4.633	34
$_1S_{32}$	5657.00 ± 8.00	5658.62		6.404	34	$_{13}S_6$		6161.19		1.541	
$_7S_{14}$		5663.80		11.200	I	$_1T_{35}$	6166.00 ± 3.50	6164.06		6.189	34
$_5S_{17}$	5669.00 + 3.00	5673.69		3.295	34	$_8S_{14}$	6169.00 ± 6.00	6170.65		3.904	34
$_2T_{24}$	5684.50 ± 4.00	5691.09		4.522	34	$_0T_{51}$		6186.78		7.628	
$_{16}S_2$		5697.12		3.042		$_9S_{12}$	6184.50 ± 2.00	6187.26		2.150	34
$_4S_{22}$	5694.00 ± 2.50	5700.49		3.861	34	$_{10}S_{10}$	6176.50 ± 2.50	6190.88		2.658	34
$_0S_{51}$	5701.20 ± 0.60	5701.42	6.99 ± .16	7.039	32	$_1S_{36}$	6200.00 ± 7.00	6203.83		6.534	34
$_4T_{16}$	5709.00 ± 7.00	5705.48		4.431	34	$_4S_{25}$	6199.00 ± 3.00	6204.82		3.868	34
$_8S_{11}$	5715.50 ± 3.00	5717.48		3.095	34	$_5T_{14}$		6217.17		4.768	
$_5T_9$		5723.92		4.943		$_{16}S_3$		6222.36		11.598	I
$_{10}S_8$	5735.00 ± 7.00	5737.09		3.550	34	$_2S_{30}$	6230.50 ± 2.50	6225.58		5.524	34
$_6S_0$	5742.00 ± 0.20	5740.25	0.90 ± .18	1.095	34	$_4T_{19}$		6234.50		4.334	
$_2S_{27}$	5736.50 ± 2.50	5745.07		5.316	34	$_6S_{18}$	6242.00 ± 2.00	6235.56		3.236	34
$_0T_{47}$		5747.66		7.631		$_0S_{57}$	6246.30 ± 1.30	6247.80	6.80 ± .13	7.357	34
$_3T_{20}$	5785.00 ± 8.00	5785.19		4.357	34	$_3S_{29}$		6270.74		2.372	M
$_1T_{32}$	5786.50 ± 3.00	5786.24		5.952	34	$_1T_{36}$	6287.50 ± 3.00	6287.87		6.263	34
$_0S_{52}$	5792.30 ± 1.20	5792.22	6.85 ± .16	7.095	32	$_0T_{52}$		6296.58		7.626	
$_1S_{33}$	5798.00 ± 6.00	5796.49		6.429	34	$_3T_{23}$	6299.00 ± 6.00	6297.60		4.491	34
$_5T_{10}$		5806.78		4.919		$_2T_{28}$	6309.50 ± 3.50	6313.75		4.667	34
$_6S_{16}$	5811.50 ± 2.50	5808.40		3.474	34	$_5S_{21}$	6312.50 ± 2.00	6316.82		3.632	34
$_{13}S_5$		5834.28		4.079		$_8S_{15}$	6306.50 ± 4.50	6317.11		3.990	34
$_5S_{18}$	5831.00 ± 3.00	5835.59		3.422	34	$_{15}S_4$		6332.35		2.507	
$_3S_{27}$		5836.74		2.389	M	$_1S_{37}$	6338.00 ± 6.00	6337.41		6.578	34
$_2T_{25}$	5843.00 ± 3.50	5848.47		4.561	34	$_0S_{58}$	6341.10 ± 1.50	6339.21	7.21 ± .16	7.406	34
$_{12}S_7$		5855.88		2.360		$_5T_{15}$		6339.76		4.713	
$_0T_{48}$	5859.00 ± 4.00	5857.43		7.631	38	$_4S_{26}$	6363.00 ± 3.50	6373.42		3.876	34
$_4S_{23}$	5858.50 ± 2.00	5868.03		3.861	34	$_2S_{31}$	6388.50 ± 2.00	6384.20		5.585	34
$_4T_{17}$	5870.00 ± 9.00	5874.88		4.396	34	$_{17}S_2$		6395.21		4.327	
$_8S_{12}$	5874.50 ± 3.50	5876.05		3.565	34	$_6T_1$		6397.86		4.955	
$_0S_{53}$	5885.00 ± 1.50	5883.13	6.83 ± .15	7.149	32	$_{13}S_7$		6398.97		2.613	
$_9S_{11}$	5887.00 ± 7.00	5885.77		2.416	34	$_{18}S_1$		6402.12		5.271	
$_5T_{11}$		5897.53		4.891		$_0T_{53}$	6408.00 ± 6.00	6406.38		7.623	38
$_2S_{28}$	5904.00 ± 2.00	5906.03		5.393	34	$_1T_{37}$	6412.50 ± 2.50	6410.74		6.333	34
$_1T_{33}$	5915.00 ± 3.50	5913.31		6.034	34	$_6T_2$		6412.65		4.948	
$_{14}S_5$		5929.81		8.644	I	$_7S_{16}$		6413.76		11.211	I
$_1S_{34}$		5933.35		6.459		$_4T_{20}$		6420.67		4.316	
$_{10}S_9$	5939.00 ± 4.50	5941.76		3.125	34	$_{19}S_1$		6427.44		11.165	I
$_3T_{21}$	5955.00 ± 6.00	5958.71		4.411	34	$_0S_{59}$	6436.30 ± 3.50	6430.72		7.454	34
$_0T_{49}$	5969.50 ± 4.00	5967.21		7.631	d	$_6T_3$		6434.81		4.938	
$_0S_{54}$	5975.60 ± 1.40	5974.14	7.15 ± .14	7.203	32	$_{11}S_9$	6437.50 ± 1.50	6437.12		1.594	34
$_5S_{19}$	5989.50 ± 2.00	5995.82		3.513	34	$_6S_{19}$	6453.50 ± 2.50	6447.44		3.197	34
$_5T_{12}$		5996.15		4.856		$_{17}S_3$		6452.27		4.679	
$_2T_{26}$	6001.00 ± 4.50	6004.65		4.598	34	$_{10}S_{11}$	6446.00 ± 6.00	6454.44		2.637	34
$_6S_{17}$	6026.50 ± 2.00	6021.31		3.325	34	$_3T_{24}$		6464.14		4.517	
$_8S_{13}$	6016.00 ± 3.50	6024.43		3.778	34	$_6T_4$		6464.29		4.924	
$_{15}S_3$	6030.96 ± 0.35	6035.22	1.24 ± .16	1.241	34	$_8S_{16}$	6471.00 ± 4.50	6464.75		4.057	34
$_4S_{24}$	6025.50 ± 3.50	6036.26		3.864	34	$_2T_{29}$	6464.50 ± 3.00	6466.83		4.698	34

TABLE 1. continued

Mode	f_{obs} μHz	f_{PREM} μHz	q_{obs}^a	q_{PREM}	ref.[b]	Mode	f_{obs} μHz	f_{PREM} μHz	q_{obs}	q_{PREM}	ref.
$_1S_{38}$	6482.00 ± 9.00	6469.86		6.627	34	$_{10}S_{13}$	6871.00 ± 9.00	6874.43		3.601	34
$_5T_{16}$		6470.62		4.651		$_4S_{29}$	6870.00 ± 2.00	6877.18		3.917	34
$_{15}S_5$		6475.31		4.113		$_0S_{64}$		6889.58		7.678	
$_5S_{22}$	6480.00 ± 6.00	6478.57		3.678	34	$_{18}S_3$	6888.00 ± 0.55	6891.93	1.21 ± .11	1.174	34
$_9S_{13}$	6487.00 ± 1.50	6483.50		2.063	34	$_1T_{41}$	6889.00 ± 6.00	6894.00		6.580	34
$_3S_{30}$		6487.70		2.368	M	$_5T_{19}$		6914.69		4.433	
$_{14}S_6$		6493.51		11.069	I	$_2T_{32}$	6911.00 ± 4.50	6920.90		4.784	34
$_6T_5$		6501.07		4.907		$_3S_{32}$		6921.36		2.363	M
$_0T_{54}$		6516.18		7.620		$_7S_{19}$	6919.00 ± 7.00	6921.84		4.175	34
$_0S_{60}$	6526.00 ± 3.00	6522.32	7.11 ± .19	7.501	34	$_{11}S_{11}$	6915.00 ± 9.00	6922.23		3.088	34
$_1T_{38}$		6532.73		6.400		$_{20}S_1$	6948.50 ± 0.60	6954.04	1.29 ± .15	1.141	34
$_4S_{27}$	6532.00 ± 2.00	6541.80		3.886	34	$_0T_{58}$	6959.00 ± 6.00	6955.42		7.604	d
$_2S_{32}$	6548.50 ± 4.00	6542.03		5.643	34	$_6T_{12}$		6956.77		4.714	
$_6T_6$		6545.07		4.887		$_3T_{27}$	6946.50 ± 3.50	6956.93		4.557	34
$_{18}S_2$		6545.69		1.876		$_5S_{25}$	6964.50 ± 3.50	6967.92		3.803	34
$_{13}S_8$		6553.59		3.591		$_4T_{23}$		6980.21		4.309	
$_{16}S_4$		6565.64		3.389		$_0S_{65}$	6985.00 ± 5.00	6981.61		7.720	d
$_7S_0$	6580.00 ± 0.50	6580.71	1.26 ± 0.09	1.135		$_1S_{42}$		6988.22		6.852	
$_{15}S_6$		6595.93		4.489		$_2S_{35}$	7015.00 ± 3.50	7010.52		5.800	34
$_6T_7$		6596.24		4.864		$_1T_{42}$	7013.50 ± 3.50	7013.05		6.633	34
$_1S_{39}$		6601.16		6.679		$_9S_{15}$	7028.00 ± 2.50	7029.82		2.325	34
$_4T_{21}$	6594.00 ± 6.00	6608.12		4.307	34	$_{10}S_{14}$	7027.00 ± 4.50	7038.76		3.859	34
$_5T_{17}$		6609.94		4.583		$_4S_{30}$	7034.00 ± 2.00	7043.91		3.938	34
$_{12}S_9$		6610.23		11.602	I	$_{14}S_8$	7039.00 ± 1.50	7047.89		2.070	34
$_0S_{61}$		6614.00		7.547		$_6S_{22}$	7053.50 ± 2.50	7048.18		3.324	34
$_7S_{17}$	6611.00 ± 4.50	6614.22		4.110	34	$_6T_{13}$		7049.19		4.680	
$_2T_{30}$	6609.00 ± 3.50	6619.02		4.728	34	$_0T_{59}$		7065.24		7.599	
$_0T_{55}$		6625.98		7.617		$_2T_{33}$	7066.00 ± 4.00	7070.65		4.811	34
$_3T_{25}$	6622.50 ± 3.50	6629.35		4.536	34	$_0S_{66}$		7073.71		7.760	
$_5S_{23}$	6635.00 ± 3.50	6641.17		3.720	34	$_{19}S_2$		7078.81		11.007	I
$_1T_{39}$	6656.00 ± 6.00	6653.89		6.464	34	$_5T_{20}$		7080.11		4.356	
$_6S_{20}$	6659.50 ± 2.00	6654.48		3.202	34	$_7S_{20}$	7085.00 ± 5.00	7081.96		4.182	34
$_6T_8$		6654.50		4.838		$_{15}S_7$		7085.82		11.488	I
$_{13}S_9$		6686.16		3.861		$_1S_{43}$		7115.01		6.914	
$_{10}S_{12}$	6682.50 ± 3.00	6687.11		3.104	34	$_3T_{28}$	7113.50 ± 3.50	7119.64		4.562	34
$_2S_{33}$		6699.04		5.698		$_5S_{26}$	7129.00 ± 2.00	7131.42		3.846	34
$_3S_{31}$		6704.57		2.365	M	$_1T_{43}$	7133.00 ± 5.00	7131.51		6.683	34
$_0S_{62}$		6705.78		7.592		$_3S_{33}$		7138.07		2.360	M
$_4S_{28}$	6705.00 ± 1.50	6709.77		3.900	34	$_{12}S_{11}$	7138.00 ± 1.50	7138.82		1.956	34
$_{11}S_{10}$	6712.50 ± 3.50	6712.42		2.345	34	$_6T_{14}$		7148.14		4.644	
$_6T_9$		6719.78		4.810		$_{11}S_{12}$	7144.00 ± 5.00	7149.61		2.725	34
$_1S_{40}$	6739.00 ± 7.00	6731.31		6.734	34	$_{16}S_6$	7149.13 ± 0.54	7153.68	1.72 ± .25	1.352	34
$_0T_{56}$		6735.79		7.613		$_{13}S_{10}$		7155.54		11.652	I
$_5T_{18}$		6757.93		4.509		$_8S_{18}$		7162.43		11.222	I
$_7S_{18}$	6764.00 ± 6.00	6766.28		4.150	34	$_4T_{24}$	7159.00 ± 8.00	7163.04		4.313	34
$_9S_{14}$	6771.50 ± 1.00	6768.24		2.063	34	$_2S_{36}$	7166.50 ± 3.00	7164.96		5.847	34
$_2T_{31}$	6763.00 ± 4.50	6770.36		4.756	34	$_0S_{67}$		7165.89		7.799	
$_{14}S_7$		6772.89		3.026		$_0T_{60}$		7175.06		7.594	
$_1T_{40}$	6773.50 ± 4.50	6774.29		6.524	34	$_{10}S_{15}$	7202.00 ± 5.00	7209.25		3.746	34
$_8S_{17}$		6788.22		11.217	I	$_4S_{31}$	7200.00 ± 2.00	7209.87		3.963	34
$_6T_{10}$		6791.98		4.780		$_2T_{34}$	7214.00 ± 6.00	7219.63		4.838	34
$_3T_{26}$	6791.00 ± 7.00	6793.54		4.548	34	$_6S_{23}$	7241.00 ± 2.00	7233.92		3.425	34
$_4T_{22}$		6795.04		4.306		$_9S_{16}$	7238.00 ± 3.00	7239.58		3.133	34
$_0S_{63}$		6797.64		7.635		$_1S_{44}$		7240.71		6.977	
$_5S_{24}$	6802.00 ± 3.00	6804.39		3.761	34	$_{18}S_4$	7238.25 ± 0.18	7241.00	1.08 ± .06	1.060	34
$_{16}S_5$	6829.84 ± 1.44	6836.41	1.86 ± .15	1.720	34	$_7S_{21}$	7238.50 ± 4.50	7247.61		4.166	34
$_0T_{57}$		6845.61		7.609		$_1T_{44}$	7249.50 ± 3.00	7249.42		6.730	34
$_{17}S_4$		6854.04		11.690	I	$_6T_{15}$		7253.56		4.609	
$_6S_{21}$	6859.00 ± 2.00	6855.03		3.246	34	$_5T_{21}$		7253.69		4.286	
$_2S_{34}$		6855.21		5.750		$_0S_{68}$		7258.14		7.838	
$_1S_{41}$		6860.33		6.792		$_3T_{29}$	7273.00 ± 4.50	7281.77		4.565	34
$_{12}S_{10}$	6860.00 ± 5.00	6861.33		3.022	34	$_0T_{61}$		7284.88		7.588	
$_6T_{11}$		6871.01		4.748		$_5S_{27}$		7294.59		3.892	

TABLE 1. continued

Mode	f_{obs} μHz	f_{PREM} μHz	q_{obs}^a	q_{PREM}	ref.[b]	Mode	f_{obs} μHz	f_{PREM} μHz	q_{obs}	q_{PREM}	ref.
$_2S_{37}$	7314.50 ± 3.50	7318.53		5.890	34	$_2T_{37}$	7653.00 ± 3.00	7661.93		4.924	34
$_4T_{25}$		7343.40		4.318		$_{15}S_8$		7664.98		11.231	I
$_0S_{69}$		7350.47		7.875		$_7T_7$		7667.63		4.741	
$_{14}S_9$	7343.94 ± 0.61	7354.08		1.892	34	$_{10}S_{17}$	7678.00 ± 1.50	7675.89		2.580	34
$_3S_{34}$		7354.71		2.358	M	$_{20}S_3$		7685.74		7.229	I
$_{20}S_2$		7357.09		1.940		$_{11}S_{14}$	7679.00 ± 3.50	7686.80		2.504	34
$_1S_{45}$		7365.35		7.041		$_{16}S_8$		7689.68		4.011	
$_6T_{16}$		7365.37		4.574		$_{13}S_{11}$		7693.02		11.669	I
$_1T_{45}$	7362.50 ± 4.50	7366.83		6.773	34	$_4T_{27}$	7694.00 ± 7.00	7697.46		4.326	34
$_2T_{35}$	7362.00 ± 4.00	7367.85		4.865	34	$_9S_{19}$	7695.00 ± 4.50	7698.29		4.030	34
$_4S_{32}$	7366.00 ± 2.00	7374.98		3.992	34	$_4S_{34}$	7691.00 ± 1.50	7702.48		4.062	34
$_0T_{62}$		7394.70		7.582		$_1T_{48}$	7713.50 ± 3.50	7716.44		6.886	34
$_9S_{17}$	7390.00 ± 5.00	7403.56		3.675	34	$_7T_8$		7717.14		4.735	
$_6S_{24}$	7418.50 ± 2.00	7413.13		3.534	34	$_0S_{73}$		7720.47		8.012	
$_{11}S_{13}$	7411.50 ± 4.00	7417.49		2.379	34	$_0T_{65}$		7724.15		7.563	
$_7S_{22}$	7416.00 ± 6.00	7419.40		4.127	34	$_1S_{48}$		7733.33		7.236	
$_{10}S_{16}$	7423.00 ± 2.50	7422.64		3.038	34	$_6T_{19}$		7738.59		4.474	
$_8S_0$	7428.00 ± 1.50	7424.13	0.90 ± .22	1.174	34	$_6S_{26}$	7756.00 ± 4.00	7757.89		3.733	34
$_5T_{22}$		7434.43		4.226		$_3T_{32}$	7757.50 ± 4.50	7764.94		4.572	34
$_0S_{70}$		7442.86		7.911		$_{15}S_9$		7771.75		4.008	
$_3T_{30}$	7439.00 ± 4.50	7443.36		4.567	34	$_7T_9$		7772.53		4.730	
$_{12}S_{12}$	7451.50 ± 2.00	7455.08		1.754	34	$_2S_{40}$	7776.00 ± 4.00	7773.95		6.005	34
$_5S_{28}$	7450.50 ± 2.00	7457.18		3.939	34	$_{12}S_{13}$	7771.00 ± 2.50	7777.00		1.758	34
$_{17}S_5$		7461.22		10.212	I	$_5S_{30}$	7776.50 ± 2.50	7780.00		4.034	34
$_2S_{38}$	7476.00 ± 4.00	7471.21		5.931	34	$_7S_{24}$	7788.00 ± 5.00	7780.08		4.013	34
$_{16}S_7$	7470.04 ± 1.00	7474.14	1.50 ± .15	1.250	34	$_3S_{36}$		7787.76		2.355	M
$_6T_{17}$		7483.49		4.540		$_{21}S_3$		7801.59		5.862	
$_1T_{46}$	7483.50 ± 4.00	7483.78		6.813	34	$_{17}S_8$		7805.05		1.838	
$_1S_{46}$		7488.98		7.106		$_2T_{38}$	7797.00 ± 4.00	7807.76		4.956	34
$_{21}S_1$		7495.27		4.718		$_5T_{24}$		7810.82		4.155	
$_7T_1$		7498.57		4.762		$_0S_{74}$		7813.15		8.043	
$_0T_{63}$		7504.52		7.576		$_{22}S_1$	7816.70 ± 0.40	7819.54	0.95 ± .05	1.304	34
$_{19}S_3$		7504.81		4.384		$_{14}S_{11}$	7803.00 ± 6.00	7823.54		3.769	34
$_7T_2$		7511.20		4.760		$_1T_{49}$	7830.00 ± 6.00	7832.22		6.918	34
$_{21}S_2$		7514.86		4.577		$_7T_{10}$		7833.70		4.725	
$_2T_{36}$	7505.00 ± 5.00	7515.28		4.894	34	$_0T_{66}$		7833.97		7.555	
$_{18}S_5$		7517.39		4.365		$_8S_{20}$	7848.00 ± 6.00	7843.35		4.106	34
$_4T_{26}$	7512.00 ± 6.00	7521.46		4.322	34	$_1S_{49}$		7854.14		7.300	
$_7T_3$		7530.11		4.758		$_4S_{35}$	7856.00 ± 1.50	7864.82		4.102	34
$_0S_{71}$		7535.33		7.946		$_4T_{28}$	7863.00 ± 8.00	7871.66		4.331	34
$_8S_{19}$		7536.41		11.229	I	$_6T_{20}$		7875.57		4.443	
$_4S_{33}$	7532.00 ± 1.50	7539.19		4.025	34	$_{15}S_{10}$	7893.00 ± 6.00	7897.49		3.224	34
$_{19}S_4$		7540.90		4.538		$_{23}S_1$		7899.09		11.631	I
$_9S_{18}$	7551.00 ± 5.00	7552.78		3.907	34	$_7T_{11}$		7900.55		4.720	
$_7T_4$		7555.27		4.754		$_0S_{75}$		7905.88		8.074	
$_3S_{35}$		7571.27		2.357	M	$_9S_{20}$		7910.21		11.235	I
$_{17}S_6$		7580.67		4.230		$_{11}S_{15}$		7919.06		3.012	
$_7T_5$		7586.61		4.750		$_2S_{41}$	7917.50 ± 6.00	7924.01		6.038	34
$_6S_{25}$	7590.00 ± 1.50	7587.27		3.640	34	$_3T_{33}$	7914.50 ± 4.50	7924.89		4.576	34
$_7S_{23}$	7598.00 ± 3.50	7597.20		4.073	34	$_6S_{27}$	7929.00 ± 7.00	7926.36		3.810	34
$_1T_{47}$	7594.00 ± 5.00	7600.31		6.851	34	$_{10}S_{18}$	7940.50 ± 2.50	7938.48		2.434	34
$_3T_{31}$	7605.00 ± 5.00	7604.42		4.569	34	$_5S_{31}$	7939.00 ± 1.50	7940.16		4.080	34
$_6T_{18}$		7607.90		4.506		$_0T_{67}$	7950.00 ± 8.00	7943.78		7.548	d
$_1S_{47}$		7611.63		7.171		$_1T_{50}$	7948.50 ± 3.50	7947.68		6.947	34
$_0T_{64}$		7614.33		7.569		$_2T_{39}$	7943.50 ± 3.00	7952.75		4.990	34
$_5S_{29}$	7616.00 ± 2.50	7619.01		3.987	34	$_{13}S_{12}$	7954.50 ± 5.50	7955.03		4.043	34
$_5T_{23}$		7620.80		4.181		$_{18}S_6$		7957.04		2.530	
$_2S_{39}$	7627.00 ± 4.00	7623.02		5.970	34	$_7S_{25}$	7968.00 ± 3.50	7966.58		3.960	34
$_7T_6$		7624.09		4.746		$_7T_{12}$		7972.96		4.715	
$_0S_{72}$		7627.87		7.979		$_1S_{50}$		7974.10		7.363	
$_{17}S_7$		7635.12		4.372		$_8S_{21}$		7989.31		4.156	
$_{14}S_{10}$	7624.00 ± 4.00	7635.75		2.574	34	$_0S_{76}$	8015.00 ± 8.00	7998.68		8.103	d
$_{19}S_5$		7661.84		2.726		$_5T_{25}$		8002.38		4.148	

TABLE 1. continued

Mode	f_{obs} μHz	f_{PREM} μHz	q^a_{obs}	q_{PREM}	ref.[b]	Mode	f_{obs} μHz	f_{PREM} μHz	q_{obs}	q_{PREM}	ref.
$_3S_{37}$		8004.19		2.353	M	$_4T_{31}$		8385.31		4.361	
$_6T_{21}$		8018.91		4.413		$_3T_{36}$	8395.00 ± 10.0	8401.09		4.598	34
$_4S_{36}$	8015.50 ± 3.50	8026.22		4.146	34	$_1T_{54}$	8400.00 ± 10.0	8406.75		7.044	34
$_4T_{29}$		8044.29		4.339		$_{12}S_{15}$	8402.00 ± 9.00	8411.28		1.840	34
$_7T_{13}$		8050.83		4.711		$_7T_{17}$		8414.71		4.696	
$_0T_{68}$		8053.59		7.540		$_5S_{34}$	8410.00 ± 4.00	8416.62		4.191	34
$_1T_{51}$	8059.00 ± 6.00	8062.83		6.975	34	$_{11}S_{18}$	8424.00 ± 8.00	8418.49		3.976	34
$_2S_{42}$	8065.00 ± 8.00	8073.21		6.069	34	$_6S_{30}$	8417.00 ± 6.00	8427.41		3.952	34
$_3T_{34}$	8080.00 ± 5.00	8084.26		4.581	34	$_{15}S_{12}$	8432.50 ± 3.00	8432.73		1.747	34
$_{13}S_{13}$		8091.46		3.907		$_3S_{39}$		8436.86		2.350	M
$_0S_{77}$		8091.55		8.131		$_{16}S_{10}$	8433.00 ± 3.00	8437.72		1.291	34
$_{19}S_6$		8093.14		10.515	I	$_8S_{24}$	8431.00 ± 8.00	8440.00		4.211	34
$_1S_{51}$		8093.25		7.425		$_1S_{54}$		8446.31		7.603	
$_6S_{28}$	8094.00 ± 5.00	8093.69		3.871	34	$_{10}S_{20}$	8451.50 ± 2.50	8446.66		2.560	34
$_2T_{40}$	8089.00 ± 5.00	8096.87		5.027	34	$_0S_{81}$		8463.61		8.232	
$_{12}S_{14}$	8093.00 ± 2.50	8097.37		1.809	34	$_{20}S_5$	8464.65 ± 0.84	8471.58		1.571	34
$_5S_{32}$	8098.00 ± 5.00	8099.56		4.122	34	$_{13}S_{15}$	8462.00 ± 9.00	8474.42		2.968	34
$_{11}S_{16}$	8100.00 ± 10.0	8107.03		3.514	34	$_6T_{24}$		8487.69		4.332	
$_{20}S_4$		8116.77		1.278		$_0T_{72}$		8492.80		7.507	
$_{16}S_9$	8116.00 ± 2.00	8117.59		1.392	34	$_4S_{39}$	8492.50 ± 3.00	8504.92		4.293	34
$_{15}S_{11}$	8132.00 ± 6.00	8130.95		1.999	34	$_2S_{45}$	8515.00 ± 8.00	8515.75		6.150	34
$_7T_{14}$		8134.04		4.707		$_7T_{18}$		8518.35		4.691	
$_8S_{22}$	8135.00 ± 8.00	8136.99		4.188	34	$_1T_{55}$		8520.94		7.063	
$_7S_{26}$	8152.00 ± 8.00	8155.16		3.919	34	$_2T_{43}$	8507.00 ± 8.00	8523.66		5.153	34
$_0T_{69}$		8163.40		7.533		$_7S_{28}$	8536.00 ± 9.00	8533.66		3.876	34
$_6T_{22}$		8168.68		4.385		$_{24}S_1$		8550.62		4.963	
$_1T_{52}$	8170.00 ± 8.00	8177.72		7.000	34	$_8T_1$		8551.15		4.975	
$_0S_{78}$		8184.47		8.158		$_4T_{32}$	8548.00 ± 7.00	8553.86		4.377	34
$_4S_{37}$	8177.50 ± 3.00	8186.69		4.192	34	$_0S_{82}$		8556.77		8.254	
$_5T_{26}$		8193.48		4.159		$_3T_{37}$	8548.00 ± 5.00	8558.49		4.609	34
$_{10}S_{19}$	8200.00 ± 3.50	8197.96		2.428	34	$_{22}S_3$		8559.91		3.686	
$_{22}S_2$		8207.04		1.397		$_{23}S_2$		8561.36		5.004	
$_1S_{52}$		8211.63		7.486		$_8T_2$		8561.68		4.974	
$_4T_{30}$	8195.00 ± 10.0	8215.47		4.348	34	$_1S_{55}$		8562.68		7.659	
$_3S_{38}$		8220.55		2.352	M	$_{11}S_{19}$		8568.59		4.020	
$_2S_{43}$	8213.00 ± 7.00	8221.56		6.098	34	$_5T_{28}$		8568.60		4.218	
$_7T_{15}$		8222.48		4.703		$_5S_{35}$	8570.50 ± 3.50	8574.62		4.218	34
$_{14}S_{12}$		8224.06		11.684	I	$_8T_3$		8577.46		4.973	
$_2T_{41}$	8230.00 ± 8.00	8240.08		5.066	34	$_{24}S_2$		8585.28		11.454	I
$_3T_{35}$		8243.00		4.589		$_6S_{31}$	8589.00 ± 5.00	8594.46		3.975	34
$_{17}S_9$		8248.53		11.488	I	$_8S_{25}$	8582.00 ± 6.00	8596.24		4.205	34
$_5S_{33}$	8253.50 ± 3.50	8258.32		4.159	34	$_{22}S_4$		8598.40		4.877	
$_{13}S_{14}$	8265.00 ± 8.00	8258.94		3.502	34	$_8T_4$		8598.47		4.970	
$_6S_{29}$	8257.50 ± 4.00	8260.57		3.918	34	$_{18}S_8$		8599.27		2.423	
$_9S_0$	8269.50 ± 1.00	8262.64	0.82 ± .20	1.190	34	$_0T_{73}$		8602.59		7.499	
$_{11}S_{17}$	8265.00 ± 8.00	8268.00		3.821	34	$_{23}S_3$		8602.59		2.605	
$_0T_{70}$		8273.20		7.524		$_8T_5$		8624.69		4.967	
$_0S_{79}$		8277.46		8.184		$_7T_{19}$		8626.95		4.685	
$_9S_{21}$		8283.85		11.241	I	$_1T_{56}$	8627.00 ± 8.00	8634.93		7.081	34
$_8S_{23}$	8273.00 ± 7.00	8287.05		4.205	34	$_{21}S_5$		8639.18		4.429	
$_1T_{53}$	8278.00 ± 7.00	8292.35		7.023	34	$_{20}S_6$		8642.79		4.644	
$_{18}S_7$		8301.04		1.444		$_0S_{83}$		8649.99		8.275	
$_7T_{16}$		8316.07		4.700		$_3S_{40}$		8653.08		2.360	M
$_6T_{23}$		8324.95		4.358		$_{25}S_1$	8652.50 ± 0.40	8655.17	1.02 ± .07	1.185	34
$_1S_{53}$		8329.31		7.545		$_8T_6$		8656.08		4.964	
$_7S_{27}$	8347.00 ± 6.00	8344.50		3.892	34	$_6T_{25}$		8656.69		4.309	
$_4S_{38}$	8336.00 ± 2.00	8346.24		4.242	34	$_9S_{22}$		8657.36		11.248	I
$_2S_{44}$	8367.00 ± 6.00	8369.08		6.124	34	$_2S_{46}$	8682.00 ± 6.00	8661.61		6.173	34
$_0S_{80}$		8370.50		8.208		$_4S_{40}$	8651.50 ± 3.00	8662.79		4.335	34
$_{21}S_4$		8373.62		11.544	I	$_2T_{44}$	8661.00 ± 9.00	8663.95		5.200	34
$_2T_{42}$	8370.00 ± 10.0	8382.36		5.108	34	$_{19}S_7$		8671.41		10.411	I
$_5T_{27}$		8382.56		4.183		$_{10}S_{21}$	8669.00 ± 4.50	8673.48		2.922	34
$_0T_{71}$		8383.00		7.516		$_1S_{56}$		8678.47		7.713	

TABLE 1. continued

Mode	f_{obs} μHz	f_{PREM} μHz	q^a_{obs}	q_{PREM}	ref.[b]	Mode	f_{obs} μHz	f_{PREM} μHz	q_{obs}	q_{PREM}	ref.
$_{12}S_{16}$	8689.50 ± 4.00	8691.79		2.225	34	$_8T_{13}$		9017.75		4.900	
$_8T_7$		8692.62		4.959		$_1S_{59}$		9022.73		7.864	
$_{20}S_7$		8706.24		5.731		$_{25}S_2$	9026.51 ± 0.69	9022.91	1.22 ± .11	1.269	34
$_0T_{74}$		8712.37		7.489		$_0S_{87}$		9023.43		8.350	
$_3T_{38}$	8697.00 ± 8.00	8715.17		4.622	34	$_3T_{40}$	9020.00 ± 10.0	9026.32		4.653	34
$_4T_{33}$	8718.00 ± 4.50	8721.15		4.395	34	$_9S_{23}$		9030.75		11.255	I
$_7S_{29}$		8722.02		3.870		$_{10}S_{23}$	9025.00 ± 10.0	9038.42		3.756	34
$_{11}S_{20}$	8715.00 ± 10.0	8726.69		3.927	34	$_0T_{77}$	9050.00 ± 8.00	9041.69		7.461	d
$_5S_{36}$	8726.50 ± 3.50	8732.50		4.237	34	$_{19}S_9$	9038.00 ± 8.00	9047.16		1.632	34
$_8T_8$		8734.26		4.953		$_5S_{38}$	9035.50 ± 4.50	9048.53		4.258	34
$_{14}S_{13}$	8724.50 ± 4.00	8734.78		2.097	34	$_4T_{35}$	9050.00 ± 5.00	9052.02		4.438	34
$_{16}S_{11}$	8729.00 ± 5.00	8736.47		1.816	34	$_{10}S_0$		9056.12		1.206	
$_7T_{20}$		8740.51		4.677		$_{13}S_{17}$	9055.50 ± 4.00	9063.12		2.083	34
$_0S_{84}$		8743.27		8.296		$_2T_{47}$	9069.00 ± 8.00	9078.56		5.359	34
$_{18}S_9$	8735.00 ± 7.00	8747.40		4.299	34	$_4S_{42}$		9085.50		2.346	M
$_1T_{57}$	8740.00 ± 10.0	8748.74		7.097	34	$_8S_{28}$		9086.85		4.143	
$_{15}S_{13}$		8749.54		11.679	I	$_1T_{60}$	9083.00 ± 9.00	9089.22		7.137	34
$_5T_{29}$		8751.14		4.257		$_8T_{14}$		9089.28		4.882	
$_{13}S_{16}$	8746.00 ± 5.00	8752.25		2.313	34	$_2S_{49}$	9093.00 ± 9.00	9094.25		6.239	34
$_8S_{26}$	8760.00 ± 9.00	8756.06		4.191	34	$_7S_{31}$	9107.00 ± 8.00	9095.12		3.875	34
$_6S_{32}$	8755.00 ± 5.00	8761.80		3.991	34	$_{16}S_{13}$		9095.71		3.627	
$_8T_9$		8780.96		4.946		$_6S_{34}$	9100.00 ± 10.0	9097.31		4.004	34
$_1S_{57}$		8793.72		7.765		$_5T_{31}$		9105.98		4.337	
$_{19}S_8$		8797.85		3.536		$_{11}S_{22}$	9101.50 ± 4.50	9111.59		3.153	34
$_2T_{45}$	8785.00 ± 6.00	8803.22		5.250	34	$_7T_{23}$		9111.72		4.629	
$_2S_{47}$		8806.64		6.196		$_0S_{88}$		9116.92		8.365	
$_{17}S_{10}$		8817.00		11.146	I	$_3S_{43}$	9120.50 ± 2.00	9131.62		4.510	34
$_3S_{41}$	8816.50 ± 2.50	8819.77		4.400	34	$_1S_{60}$		9136.57		7.911	
$_0T_{75}$		8822.15		7.480		$_{12}S_{18}$		9145.99		3.073	
$_6T_{26}$		8831.46		4.290		$_{17}S_{12}$	9146.00 ± 5.00	9151.28		2.163	34
$_8T_{10}$		8832.70		4.937		$_0T_{78}$		9151.46		7.451	
$_{18}S_{10}$		8836.23		4.985		$_8T_{15}$		9165.71		4.862	
$_0S_{85}$		8836.60		8.315		$_{14}S_{15}$		9168.47		3.598	
$_{21}S_6$	8848.57 ± 0.71	8850.77	1.60 ± .20	1.351	34	$_{21}S_7$	9167.79 ± 0.53	9173.79	1.58 ± .20	1.250	34
$_7T_{21}$		8859.08		4.665		$_3T_{41}$	9166.00 ± 8.00	9180.76		4.670	34
$_1T_{58}$	8851.00 ± 9.00	8862.38		7.112	34	$_6T_{28}$		9194.29		4.271	
$_{10}S_{22}$	8868.00 ± 7.00	8868.46		3.417	34	$_9S_{24}$	9175.00 ± 10.0	9196.93		3.929	34
$_4S_{41}$		8869.34		2.348	M	$_1T_{61}$	9197.00 ± 8.00	9202.44		7.148	34
$_3T_{39}$	8858.00 ± 8.00	8871.12		4.637	34	$_5S_{39}$	9195.00 ± 4.50	9206.92		4.259	34
$_4T_{34}$	8873.00 ± 6.00	8887.20		4.416	34	$_0S_{89}$		9210.47		8.380	
$_8T_{11}$		8889.44		4.927		$_2T_{48}$	9204.00 ± 8.00	9214.61		5.416	34
$_5S_{37}$	8882.50 ± 2.00	8890.43		4.250	34	$_4T_{36}$	9210.00 ± 8.00	9215.65		4.462	34
$_{11}S_{21}$		8904.37		3.606		$_{24}S_3$		9218.64		10.287	I
$_1S_{58}$		8908.46		7.816		$_2S_{50}$		9236.83		6.261	
$_7S_{30}$		8909.23		3.870		$_7T_{24}$		9246.21		4.601	
$_8S_{27}$	8912.00 ± 6.00	8919.60		4.170	34	$_8T_{16}$		9247.01		4.839	
$_6S_{33}$	8929.00 ± 6.00	8929.44		4.000	34	$_1S_{61}$		9250.01		7.955	
$_0S_{86}$	8955.00 ± 8.00	8929.99		8.333	d	$_8S_{29}$	9258.00 ± 9.00	9257.65		4.114	34
$_5T_{30}$		8930.17		4.298		$_0T_{79}$		9261.21		7.441	
$_0T_{76}$		8931.93		7.471		$_{20}S_8$		9262.17		11.298	I
$_{12}S_{17}$	8929.00 ± 5.00	8933.91		2.612	34	$_6S_{35}$		9265.32		4.006	
$_2T_{46}$	8932.00 ± 7.00	8941.43		5.303	34	$_{15}S_{14}$		9270.16		11.706	I
$_{23}S_4$	8934.36 ± 0.70	8941.57	1.34 ± .15	1.235	34	$_5T_{32}$		9279.00		4.372	
$_{17}S_{11}$		8942.70		3.946		$_7S_{32}$		9279.63		3.882	
$_{16}S_{12}$		8944.33		3.522		$_3S_{44}$	9275.00 ± 3.50	9286.52		4.564	34
$_2S_{48}$	8955.00 ± 10.0	8950.86		6.218	34	$_{23}S_5$	9289.53 ± 0.30	9289.58	1.12 ± .17	1.112	34
$_8T_{12}$		8951.13		4.914		$_4S_{43}$		9301.61		2.345	M
$_1T_{59}$		8975.87		7.125		$_0S_{90}$		9304.07		8.394	
$_3S_{42}$	8966.50 ± 2.50	8976.05		4.455	34	$_{16}S_{14}$		9304.36		2.698	
$_7T_{22}$		8982.76		4.650		$_1T_{62}$	9307.00 ± 7.00	9315.53		7.157	34
$_{14}S_{14}$	8978.00 ± 6.00	8985.12		3.019	34	$_{12}S_{19}$	9341.00 ± 8.00	9329.10		3.469	34
$_{22}S_5$		9005.25		11.708	I	$_8T_{17}$		9333.20		4.813	
$_6T_{27}$		9011.09		4.277		$_3T_{42}$	9323.00 ± 8.00	9334.44		4.688	34

TABLE 1. continued

Mode	f_{obs} μHz	f_{PREM} μHz	q_{obs}^a	q_{PREM}	ref.[b]	Mode	f_{obs} μHz	f_{PREM} μHz	q_{obs}	q_{PREM}	ref.
$_{14}S_{16}$		9337.18		3.543		$_9T_4$		9621.48		4.773	
$_{11}S_{23}$	9333.00 ± 5.00	9341.10		2.863	34	$_3T_{44}$	9615.00 ± 7.00	9639.58		4.723	34
$_2T_{49}$	9333.00 ± 8.00	9349.55		5.475	34	$_7S_{34}$	9651.00 ± 5.00	9644.54		3.899	34
$_9S_{25}$		9351.55		4.017		$_9T_5$		9645.80		4.762	
$_{19}S_{10}$	9343.00 ± 5.00	9357.39		1.479	34	$_{23}S_6$		9646.41		7.094	I
$_1S_{62}$		9363.08		7.997		$_{12}S_{21}$	9646.00 ± 7.00	9647.81		3.867	34
$_{26}S_1$		9364.82		11.554	I	$_{24}S_5$		9647.92		4.675	
$_5S_{40}$	9353.50 ± 3.00	9365.67		4.256	34	$_{19}S_{11}$		9653.75		1.872	
$_0T_{80}$		9370.95		7.430		$_1T_{65}$	9648.00 ± 4.00	9654.15		7.180	34
$_{13}S_{18}$	9366.00 ± 6.00	9371.79		2.038	34	$_2S_{53}$		9659.62		6.326	
$_4T_{37}$	9390.00 ± 7.00	9378.12		4.485	34	$_9S_{27}$		9660.38		4.088	
$_2S_{51}$		9378.59		6.282		$_{13}S_{19}$	9668.00 ± 7.00	9671.80		2.054	34
$_6T_{29}$		9379.50		4.272		$_9T_6$		9674.96		4.750	
$_{18}S_{11}$		9384.31		11.660	I	$_0S_{94}$		9678.99		8.438	
$_7T_{25}$		9386.54		4.564		$_5S_{42}$	9666.00 ± 3.00	9684.42		4.239	34
$_0S_{91}$		9397.73		8.407		$_7T_{27}$		9686.26		4.465	
$_{10}S_{24}$		9404.05		11.263	I	$_4T_{39}$	9679.00 ± 9.00	9699.82		4.530	34
$_8T_{18}$		9424.29		4.783		$_0T_{83}$		9700.14		7.398	
$_{25}S_3$		9424.61		2.646		$_{24}S_6$		9700.17		4.089	
$_1T_{63}$	9420.00 ± 10.0	9428.51		7.166	34	$_1S_{65}$		9700.36		8.113	
$_8S_{30}$	9413.00 ± 9.00	9431.74		4.083	34	$_9T_7$		9708.96		4.735	
$_6S_{36}$	9420.00 ± 6.00	9433.35		4.005	34	$_{17}S_{14}$	9705.00 ± 6.00	9709.08		2.165	34
$_{17}S_{13}$	9430.00 ± 6.00	9435.93		1.804	34	$_{22}S_7$		9716.00		4.489	
$_3S_{45}$	9424.00 ± 4.50	9440.80		4.618	34	$_8T_{21}$		9727.24		4.671	
$_5T_{33}$		9449.69		4.402		$_4S_{45}$		9733.71		2.343	M
$_7S_{33}$	9464.00 ± 9.00	9462.76		3.890	34	$_3S_{47}$	9729.00 ± 6.00	9747.60		4.724	34
$_1S_{63}$		9475.81		8.038		$_9T_8$		9747.78		4.719	
$_0T_{81}$		9480.69		7.420		$_2T_{52}$	9745.00 ± 10.0	9747.83		5.661	34
$_2T_{50}$	9475.00 ± 10.0	9483.40		5.536	34	$_{14}S_{18}$	9725.00 ± 10.0	9748.85		2.707	34
$_{27}S_1$	9484.00 ± 0.50	9485.84	1.35 ± .24	1.542	34	$_{25}S_4$		9749.46		3.347	
$_3T_{43}$	9472.00 ± 7.00	9487.38		4.706	34	$_6T_{31}$		9750.03		4.287	
$_0S_{92}$		9491.43		8.418		$_1T_{66}$		9766.83		7.187	
$_{12}S_{20}$	9486.00 ± 9.00	9493.18		3.724	34	$_{22}S_8$		9766.99		4.488	
$_{21}S_8$	9489.93 ± 1.20	9496.96	1.50 ± .09	1.497	34	$_6S_{38}$		9768.94		4.004	
$_9S_{26}$	9502.00 ± 8.00	9505.55		4.063	34	$_0S_{95}$		9772.85		8.447	
$_4S_{44}$		9517.68		2.344	M	$_{10}S_{25}$		9777.27		11.271	I
$_2S_{52}$	9538.00 ± 8.00	9519.52		6.304	34	$_5T_{35}$		9785.86		4.443	
$_8T_{19}$		9520.30		4.749		$_{16}S_{15}$		9786.62		11.714	I
$_5S_{41}$	9512.50 ± 4.50	9524.84		4.249	34	$_8S_{32}$		9788.23		4.023	
$_{14}S_{17}$		9526.65		3.162		$_{20}S_9$	9810.00 ± 10.0	9790.64		3.485	34
$_7T_{26}$		9533.08		4.519		$_3T_{45}$	9782.00 ± 9.00	9791.08		4.741	34
$_4T_{38}$		9539.49		4.509		$_9T_9$		9791.40		4.700	
$_1T_{64}$	9539.00 ± 8.00	9541.38		7.174	34	$_2S_{54}$	9820.00 ± 10.0	9798.87		6.348	34
$_6T_{30}$		9565.17		4.279		$_{12}S_{22}$		9799.02		3.939	
$_9T_1$		9577.68		4.792		$_0T_{84}$		9809.85		7.387	
$_{11}S_{24}$	9576.50 ± 4.50	9578.38		2.757	34	$_1S_{66}$		9812.22		8.148	
$_{28}S_1$		9579.07		4.744		$_{11}S_{25}$	9811.00 ± 5.00	9814.25		2.769	34
$_0S_{93}$		9585.19		8.429		$_9S_{28}$		9816.78		4.100	
$_{26}S_2$		9586.48		4.754		$_7S_{35}$	9827.00 ± 9.00	9824.99		3.908	34
$_9T_2$		9587.42		4.788		$_{21}S_9$		9828.72		4.309	
$_1S_{64}$		9588.23		8.077		$_8T_{22}$		9838.26		4.626	
$_0T_{82}$		9590.42		7.409		$_9T_{10}$		9839.82		4.680	
$_3S_{46}$	9575.50 ± 4.50	9594.48		4.672	34	$_5S_{43}$	9826.00 ± 7.00	9844.43		4.227	34
$_{15}S_{15}$	9599.00 ± 7.00	9597.78		2.004	34	$_7T_{28}$		9846.40		4.402	
$_6S_{37}$	9597.50 ± 6.50	9601.27		4.005	34	$_4T_{40}$		9859.20		4.550	
$_9T_3$		9602.02		4.781		$_{27}S_2$	9869.31 ± 1.00	9865.33	1.32 ± .10	1.266	34
$_{22}S_6$		9603.76		6.315		$_0S_{96}$		9866.75		8.455	
$_{26}S_3$		9604.98		4.727		$_{22}S_9$		9871.01		9.425	I
$_8S_{31}$	9596.00 ± 8.00	9608.74		4.052	34	$_2T_{53}$		9878.43		5.725	
$_{24}S_4$		9615.50		4.537		$_1T_{67}$		9879.42		7.192	
$_2T_{51}$	9615.00 ± 10.0	9616.16		5.598	34	$_{11}S_0$		9887.92		1.202	
$_5T_{34}$		9618.51		4.426		$_9T_{11}$		9893.01		4.658	
$_8T_{20}$		9621.27		4.712		$_{18}S_{12}$		9894.79		2.975	

TABLE 1. continued

Mode	f_{obs} μHz	f_{PREM} μHz	q^a_{obs}	q_{PREM}	ref.[b]	Mode	f_{obs} μHz	f_{PREM} μHz	q_{obs}	q_{PREM}	ref.
$_{20}S_{10}$		9900.15		4.259		$_4S_{46}$		9949.71		2.343	M
$_3S_{48}$	9877.00 ± 6.00	9900.17		4.775	34	$_{12}S_{23}$		9950.43		3.965	
$_{26}S_4$		9910.84		9.693	I	$_9T_{12}$		9950.95		4.634	
$_0T_{85}$	9930.00 ± 10.0	9919.55		7.376	d	$_5T_{36}$		9952.11		4.453	
$_1S_{67}$		9923.84		8.182		$_8T_{23}$		9954.41		4.579	
$_{15}S_{16}$		9926.89		1.857		$_0S_{97}$	9998.00 ± 10.0	9960.70		8.461	d
$_6T_{32}$		9933.27		4.293		$_{13}S_{20}$		9961.02		2.114	
$_6S_{39}$		9936.22		4.004		$_8S_{33}$		9969.78		3.997	
$_2S_{55}$		9937.26		6.372		$_9S_{29}$		9975.13		4.106	
$_{17}S_{15}$		9938.07		2.835		$_{23}S_7$		9983.94		1.497	
$_3T_{46}$	9926.00 ± 7.00	9941.90		4.758	34	$_1T_{68}$		9991.93		7.197	
$_{19}S_{12}$		9945.85		11.627	I	$_{14}S_{19}$		9994.61		2.461	

a) $q \equiv 1000/Q$;   b) Reference number or mode type;   c) Coriolis or second order rotation correction applied.
d) Preliminary estimates from surface-wave dispersion (see text)
I denotes a mode a mode whose energy is trapped within the inner core or on the inner-core boundary (unlikely to be observed).
M denotes a Stoneley mode trapped on the core-mantle boundary (unlikely to be observed).
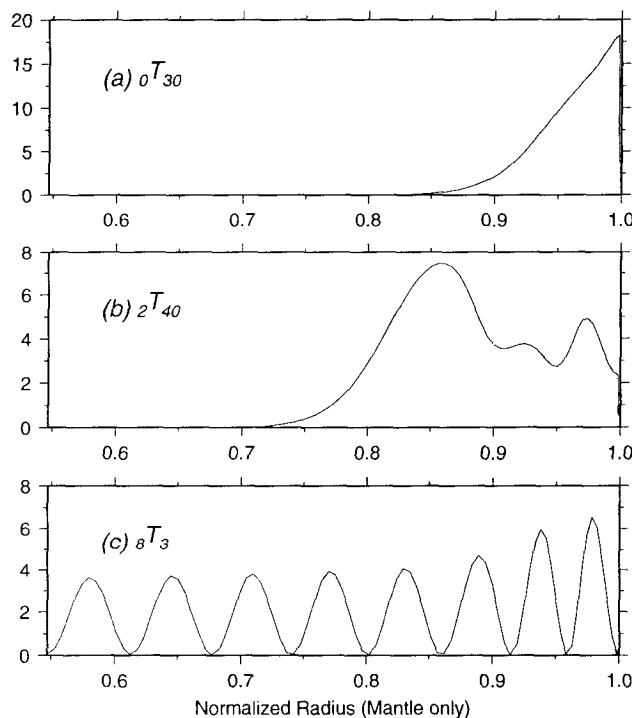
Fig. 5. Shear-energy density as a function of radius in the mantle (R = 1 is the surface). The energy has been normalized so that the total potential energy of the mode is unity. Panel (a) is a fundamental toroidal mode demonstrating how surface-wave equivalent modes have their sensitivity concentrated near the surface of the Earth. Panel (b) is a "mantle S-equivalent" mode - the turning point is at about R = 0.85. Panel (c) is an "ScS-equivalent" mode which is oscillatory throughout the mantle.

modes in the upper left triangle of Figure 4 are like this and, when added together using equation (1), make a seismogram which corresponds to the body wave arrival ScS and its multiples. Such modes are called "ScS-equivalent". Adding all the modes together gives a complete seismogram.

A similar analysis can be carried out for spheroidal modes and Figure 6 shows the elastic compressional and shear energy densities for a variety of modes. Since spheroidal modes are not confined to the mantle, it is now possible to get modes which are interface waves trapped at the core mantle boundary and the inner core boundary. Such modes are called Stoneley modes. Fundamental spheroidal modes are the free-surface equivalent of these and are called surface-wave equivalent modes (Rayleigh waves). Other modes are considered to be equivalent to various kinds of body waves depending upon the location of their turning points and the distributions of compressional and shear energy. It is the great variety of ways in which free oscillations sample the Earth that makes them extremely powerful at constraining the structure of the Earth.

Returning to Figure 3, the clear large-amplitude peaks which are roughly evenly spaced in frequency about 0.1 mHz apart are fundamental spheroidal modes which comprise the large amplitude surface waves in the time domain. Figure 3 is typical for the spectrum of a shallow event. By way of contrast, Figure 7 shows the spectrum of the Payson recording of the deep 1970 Columbian earthquake which, because of the absence of fundamental modes, is completely dominated by overtones. Each peak in Figure 3 and 7 is actually a multiplet composed of $2\ell + 1$ singlets. The singlets are too close together to be resolved since they are broadened by attenuation and finite record
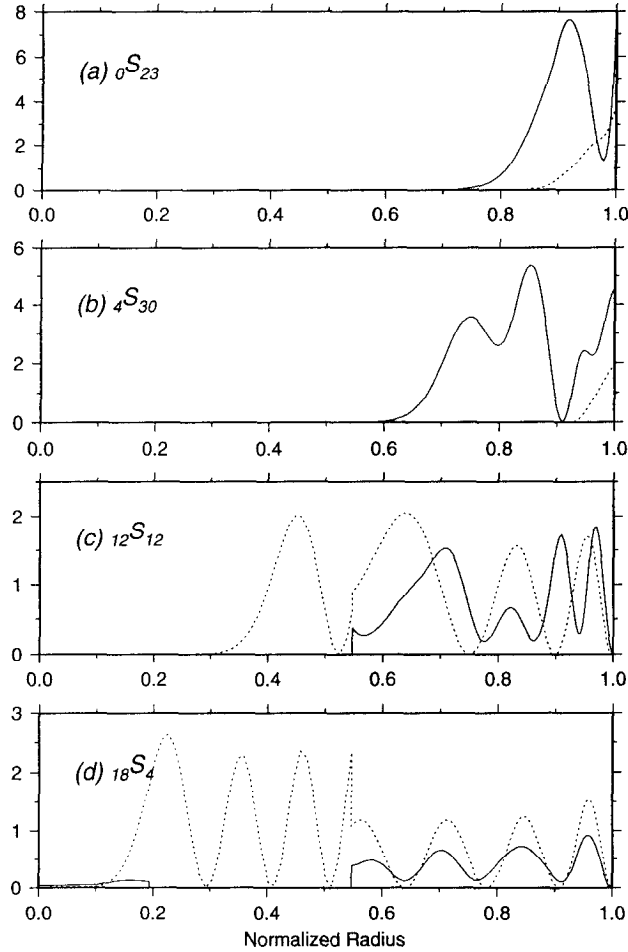
Fig. 6. Shear-energy density (solid line) and compressional energy density (dashed line) for selected spheroidal modes. Panel (a) is a surface-wave equivalent mode, panel (b) is a mantle S-equivalent mode, panel (c) is a PKP-equivalent mode, and panel (d) is a $PKIKP$-equivalent mode. Note that the inner-core boundary is at a normalized radius of 0.19 and the core-mantle boundary is at a normalized radius of 0.55.

length effects. This is not always the case, particularly if we choose low ℓ, high Q multiplets since there are then only a few narrow peaks. Very-low frequency modes are also resolvably split because of their strong sensitivity to the rotation of the Earth (Figure 8).

A traditional way of measuring mode frequencies involves simply picking the peak of the Fourier amplitude spectrum. This can lead to bias if there are nearby interfering modes and also gives no estimate of error. Similarly, the traditional way of measuring attenuation is to perform a "time lapse" analysis where the amplitude of a mode is
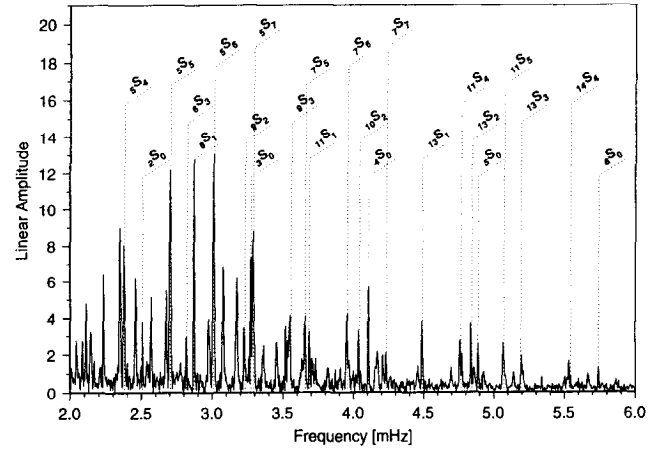
Fig. 7. Linear amplitude spectrum of 67 hours of recording of the large 1970 Colombian earthquake (depth 650 km) made by a modified LaCoste gravimeter sited at Payson, Arizona. This event was too deep to excite large surface waves so the spectrum is very different from that of Figure 3. Nearly all peaks are overtone modes of oscillation some of which (e.g., $_{11}S_1$) have not been strongly excited since.
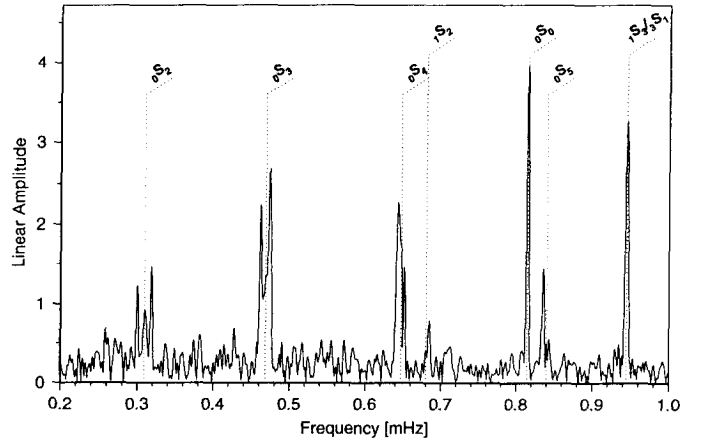
Fig. 8. A spectrum of 150 hours of recording of the 1977 Sumbawa earthquake (the largest earthquake to be digitally recorded since 1975) at station BDF (Brazilia). The very-low frequency part of the spectrum is shown illustrating that the multiplets are now visibly split into multiple peaks. In this frequency band, the "splitting" is dominantly due to the rotation of the Earth. The multiplets $_1S_3$ and $_3S_1$ overlap in frequency.

measured from the spectra of successive time windows and attenuation is estimated from the resulting amplitude decay. It turns out that this method is also biased if there are nearby modes and is an inefficient estimator (in a statistical sense) of the attenuation rate. Several methods which can simultaneously estimate the properties of closely spaced modes have been developed [21, 5, 17]. An example of simple least-squares fitting of a resonance function to the observed spectrum using an iterative technique is shown in Figure 9 where the original amplitude spectrum around a mode of interest is shown along with a residual spectrum after removal of the best-fitting resonance function. An alternative technique based upon the autoregressive character of equation (1) allows determination of a mode frequency and decay rate in a single step.

Most of the Q measurements given in Table 1 are the means of many hundreds of mode measurements. The reason that we must use many measurements to get an accurate estimate of the mean attenuation rate is that the spectral width of a multiplet is greatly influenced by the interference between singlets within that multiplet due to the splitting caused by 3-dimensional structure. The values in Table 1 are based on the assumption that the mean width of the multiplet is related to the attenuation rate that the multiplet would have if it were not split. There is some theoretical justification for this [7] and it seems to be supported by experiments with synthetic data [8] though there is still some controversy as to whether the resulting Q values are unbiased [10].

Most of the techniques discussed above are capable of simultaneous estimation of the properties of more than one mode from a single recording. This is useful but there are often severe tradeoffs when multi-mode estimation is attempted. To circumvent this, we often add records together in various ways to enhance a particular mode of interest. Consider equation (1) but now written in the frequency domain as

$$u_j(\omega) = \sum_k a_{kj} C_k(\omega) \qquad (3)$$

where a_{kj} is a complex number with

$$A_k = |a_{kj}| \quad \text{and} \quad \phi_k = \tan^{-1}\left[\frac{Im(a_{kj})}{Re(a_{kj})}\right]$$

and $C_k(\omega)$ is the spectrum of a decaying cosinusoid. We have used the j index to indicate that this recording is for the j'th source-receiver pair. Suppose we have many recordings of a multiplet at a particular frequency ω and suppose we can estimate the initial amplitude and phase
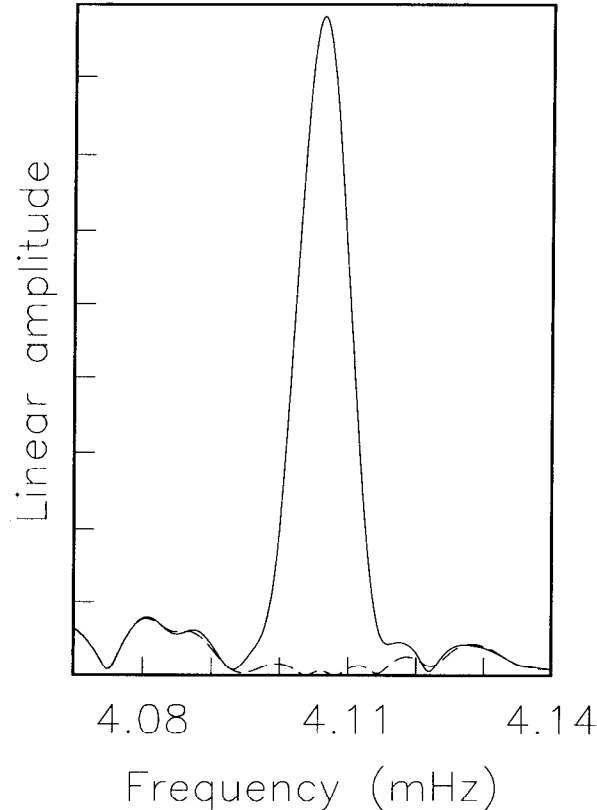
Fig. 9. A close-up of the spectrum shown in Figure 7 around the mode $_4S_0$. The dashed line shows the residual after the best-fitting resonance function has been fit to the data. This process gives a center frequency of 4.1062 mHz and a Q value of 1210.

of the k'th mode (A_{kj}, ϕ_{kj}) based on a model of the source mechanism. We can then use the equation to estimate the resonance function of the k'th mode at frequency ω:

$$\mathbf{C}(\omega) = \mathbf{a}^{-1}\mathbf{u}(\omega) \qquad (4)$$

Solving this system at a number of frequencies in a narrow frequency band encompassing several modes allows the resonance function of those modes to be estimated (Figure 10). The properties of those modes (e.g. center frequency and decay rate) can then be determined from the recovered resonance functions. This technique, called "stripping" by Gilbert and Dziewonski [16], can be applied to isolate singlets within multiplets as well as to isolate multiplets from other multiplets. Most of the multiplet frequencies given in Table 1 were measured from strips of several thousands of recordings.
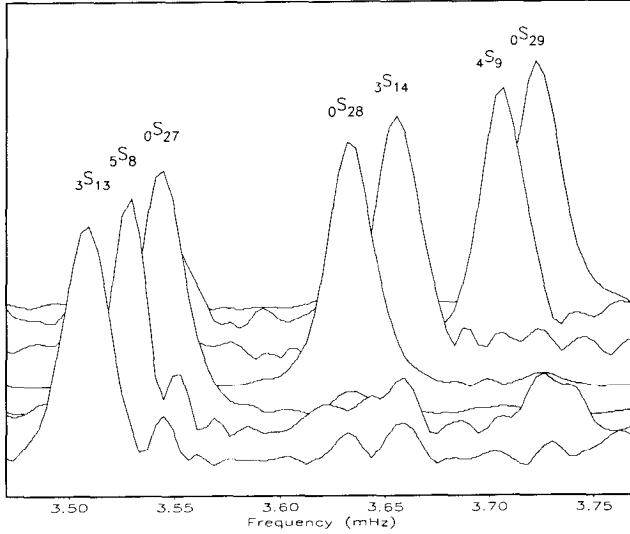
Fig. 10. The results of multiplet stripping in a small frequency band which includes the fundamental spheroidal modes $_0S_{27}$ and $_0S_{28}$. The target multiplets are (front to back) $_3S_{13}$, $_5S_8$, $_0S_{27}$, $_0S_{28}$, $_3S_{14}$, $_4S_9$ and $_0S_{29}$. Note that overtones such as $_3S_{14}$ are clearly separated from the highly excited fundamental modes.

3. MODE SPLITTING AND COUPLING

A theoretical treatment of mode splitting and coupling is beyond the scope of this paper but this section tries to give a flavor of the effects upon the observations and, in particular, how they can bias degenerate frequency estimates.

For many purposes, coupling between multiplets is sufficiently weak to be neglected and we can consider the mode to be "isolated". We divide the splitting of isolated multiplets up into two categories: 1) resolvably split multiplets where we can attempt to isolate individual singlets of a multiplet and 2) unresolvably split multiplets where it is not possible to analyze individual singlets but the spectrum of a multiplet varies in a systematic way depending upon source/receiver orientation. All fundamental modes above about $\ell = 10$ fall in the latter category since there are so many broad singlets in the multiplet which completely overlap in the frequency domain. Inspection of several recordings of an unresolvably split multiplet reveals that the multiplet looks like a single resonance function but the peak appears to move around. Theoretical work in the late 70's showed that the phenomenon is a result of interference between the singlets within the multiplet and that the apparent peak frequency is dominantly a function of the structure underlying the great circle joining source

and receiver. Thus, the spectral peak of a multiplet for a fast great-circle path is at an apparently high frequency while a slow great-circle path produces a low frequency peak. In the limit that the wavelength of the structure is much longer than the wavelength of the multiplet, Jordan [18] showed that the observed peak shift is given by:

$$\delta\omega = \sum_s P_s(0) \sum_t c_s^t Y_s^t(\Theta, \Phi) \tag{5}$$

where the c_s^t are the so-called "structure coefficients" and the Y_s^t are spherical harmonics defined in equation (12). Θ and Φ are the colatitude and longitude of the pole of the great circle joining the source and receiver. Plotting the peak shift of a multiplet for many different recordings at the appropriate great-circle pole positions reveals a large-scale pattern [22] which is dominated by structure of harmonic degree 2 (Figure 11).

The structure coefficients are simply related to 3-dimensional structure. In particular, if 3-dimensional structure is expanded as

$$m(r, \theta, \phi) = \bar{m}(r) + \delta m(r, \theta, \phi) \tag{6}$$

where

$$\delta m(r, \theta, \phi) = \sum_{s,t} \delta m_s^t(r) Y_s^t(\theta, \phi)$$

and $\bar{m}$ is the spherically averaged model then the structure coefficients are related to the model expansion coefficients by an equation of the form:

$$c_s^t = \int_0^a M_s(r) \delta m_s^t(r) r^2 dr \tag{7}$$

(See Woodhouse and Dahlen [39] for the form of the integral kernels M_s.) Clearly, observations of peak shifts can be used to determine structure coefficients which in turn can be inverted for the 3-dimensional structure expansion coefficients [e.g., 33]. Unfortunately, multiplet peak shift data can constrain only the even degree ($s = 2, 4, 6...$) part of the structure. This is because the mode spectrum includes many orbits of surface waves and such data effectively average out the odd-degree part of the 3-dimensional structure. Using equation (5) to find structure coefficients which fit the observed peak shifts also results in refined estimates of the degenerate frequency and it is these frequencies which are given in Table 1 when available.

One final comment about Table 1 is necessary. Explicit accounting for the effects of 3-dimensional structure as in the studies described above can lead to extremely precise
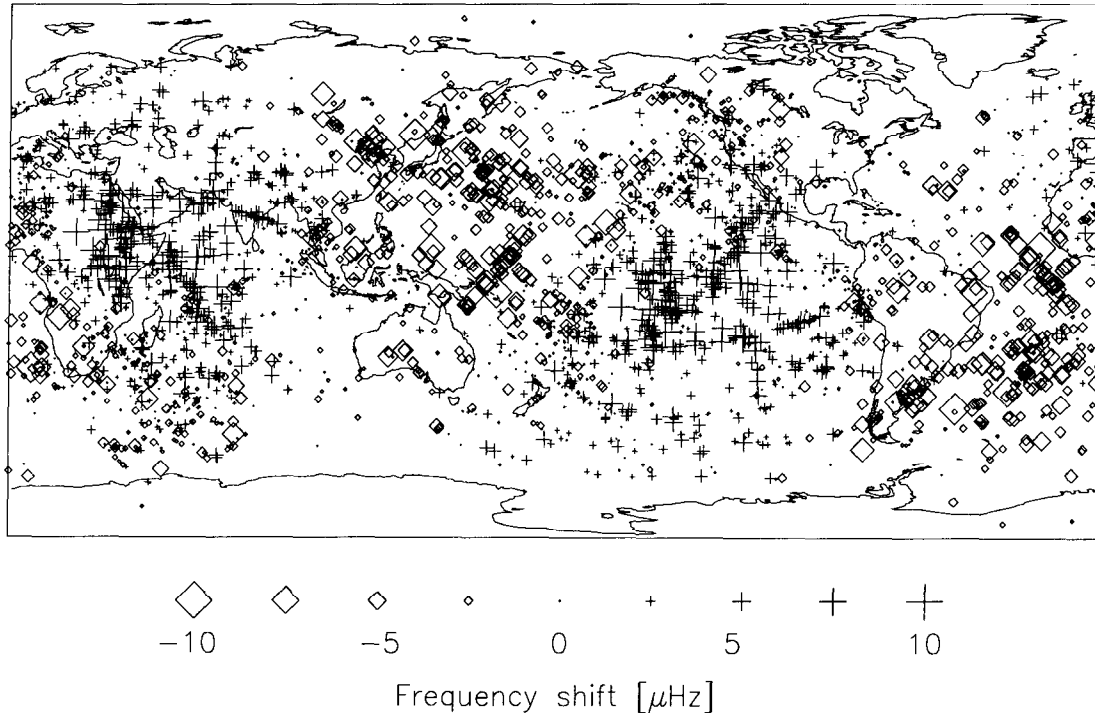
Fig. 11. Fundamental mode peak shifts for the mode $_0S_{23}$ from Smith and Masters [33]. The symbols are plotted at the pole of the great circle joining the source and the receiver locations. Plus symbols (+) indicate an anomalously high frequency corresponding to a fast great-circle path on average. Converseley diamonds (◇) plot at the poles of slow great-circle paths. The size of the symbols reflects the magnitude of the frequency shift which varies by $\pm 10\mu$Hz. Note the coherent degree 2 pattern which is caused by 3D-structure in the upper mantle and transition zone.

mean frequency estimates for a multiplet but it is not always true that this is a reliable estimate of the degenerate frequency of the multiplet. The reason is that coupling of one mode to another through rotation or 3-dimensional structure can lead to an effective shifting of the mean frequency. A clear example of mode-coupling is the coupling of toroidal fundamental modes to spheroidal fundamental modes in the frequency band 1.8 – 3.3 mHz by the Coriolis force [23]. In this case, the shift of the apparent mode frequency can be computed and the data in Table 1 have been corrected for this effect.

4. SUMMARY

Table 1 represents our latest compilation of reliable degenerate frequency estimates. One single method cannot give accurate degenerate frequencies for all modes and, in fact, we have used four methods of degenerate frequency estimation:

1) Histogram analysis of peak-frequency measurements from single recordings. The measurements must be corrected for the signal from 3-dimensional structure [31, 21, 29, 28, 8, 33, 32, 30].

2) Multiple-record analysis to isolate the individual singlets of a multiplet so that a reliable mean can be estimated [4, 26, 36, 39].

3) Fitting of the spectra of split multiplets including the effects of aspherical structure as well as a perturbation to the degenerate frequency [14,15, 26, 27, 20, 36, 39].

4) Multiple-record analysis ignoring 3-dimensional structure [16, 34].

Many of our measurements have been determined using more than one of these techniques allowing some sources of bias to be estimated. Slightly over 600 mode frequencies are listed which is significantly less than the 1064 frequencies reported by Gilbert and Dziewonski [16]. Some of the high-frequency fundamental toroidal and spheroidal measurements are absent from the current list since precise mean values from a global study are not yet available. Several research groups are actively studying global

surface-wave dispersion and we give some preliminary values based on the results of Wong [38] and unpublished results of Dr J-P. Montagner and of Dr. G. Laske. Also missing are degenerate frequency estimates for some high Q, low-ℓ modes which were originally identified using a simple histogram analysis [12, 13]. Strong splitting of such modes is very common and great care must be taken to get unbiased degenerate frequency estimates. It will probably take another earthquake like the 1970 Columbian event before we have the recordings to significantly expand the dataset.

5. APPENDIX

This appendix describes some basic theoretical results – a more complete treatment can be found in Lapwood and Usami [19].

Since departures from spherical symmetry are small (particularly in the deep Earth), it is useful to consider an approximate Earth model which is spherically symmetric, non-rotating, and elastically isotropic. Departures from this state (i.e. anelasticity, anisotropy, rotation and three-dimensional structure) are supposed sufficiently small that they can be treated by perturbation theory. The model is assumed to be initially quiescent and in a state of hydrostatic equilibrium. The equations governing the small oscillations of such a body are given by:

$$\rho_0 \frac{\partial^2 \mathbf{s}}{\partial t^2} = \nabla \cdot \mathbf{T} - \nabla(s_r \rho_0 g_0) - \rho_0 \nabla \phi_1 + \hat{\mathbf{r}} g_0 \nabla \cdot (\rho_0 \mathbf{s}) + \mathbf{f} \quad (8)$$

and

$$\nabla^2 \phi_1 = -4\pi G \nabla \cdot (\rho_0 \mathbf{s}) \quad (9)$$

Equation (8) is the linearized equation for conservation of momentum. ρ_0 is the unperturbed density and $\mathbf{s}$ is the displacement field. The acceleration due to gravity is given by $\mathbf{g}(r) = -\hat{\mathbf{r}} g_0(r)$, $\mathbf{T}$ is the elastic stress tensor and $\mathbf{f}$ is a body force density used to represent the earthquake source ($\mathbf{f} = 0$ when the Earth is in free oscillation). Since the motion of the earth causes a disturbance of the gravitational potential which in turn affects the motion, we must also solve Poisson's equation (equation 9) where ϕ_1 is the perturbation in the gravitational potential associated with the motion. Considering the linearized the momentum equation, the force densities contributing to the acceleration of material at a fixed point in space are respectively: 1) elastic forces caused by the deformation of the body, 2) motion of material in the initial stress field, 3) forces due

to the change in gravitational potential, and 4) forces due to motion within the initial gravitational field.

We seek solutions to equation 8 and 9 which satisfy certain boundary conditions on the displacement field and the tractions acting on interfaces (the traction acting on a surface with normal $\hat{\mathbf{n}}$ is $\mathbf{T} \cdot \hat{\mathbf{n}}$). In particular, the displacement field must be continuous everywhere except at a fluid-solid boundary where slip is allowed. The tractions on horizontal surfaces must be continuous at all interfaces and must vanish at the free surface. The usual way to proceed is to use separation of variables and expand the displacement field in vector spherical harmonics. We recognize that there may be more than one solution to equation 8 and 9 and designate the k'th solution by $\mathbf{s}_k$ where:

$$\mathbf{s}_k = \hat{\mathbf{r}} \,_k U + \nabla_1 \,_k V - \hat{\mathbf{r}} \times (\nabla_1 \,_k W) \quad (10)$$

$\nabla_1 = \hat{\boldsymbol{\theta}} \partial_\theta + \hat{\boldsymbol{\phi}} \operatorname{cosec} \theta \partial_\phi$ is the horizontal gradient operator and $_k U$, $_k V$ and $_k W$ are scalar functions of position. We now expand $_k U$, $_k V$ and $_k W$ in ordinary spherical harmonics as well as ϕ_{1k}. Each of these functions have an expansion of the form

$$\left. \begin{aligned} _k U &= \sum_{l=0}^{\infty} \sum_{m=-l}^{l} {}_k U_l^m(r) Y_l^m(\theta, \phi) \\ _k V &= \sum_{l=0}^{\infty} \sum_{m=-l}^{l} {}_k V_l^m(r) Y_l^m(\theta, \phi), \quad \text{etc.} \end{aligned} \right\} \quad (11)$$

where the $Y_l^m(\theta, \phi)$ are fully normalized spherical harmonics:

$$Y_l^m(\theta, \phi) = (-1)^m \left[\frac{2l+1}{4\pi} \frac{(l-m)!}{(l+m)!} \right]^{\frac{1}{2}} P_l^m(\cos\theta) e^{im\phi} \quad (12)$$

and the P_l^m are associated Legendre functions.

To proceed, we adopt a constitutive relation for the material to relate $\mathbf{T}$ to the deformation of the body. In the simplest case, a perfectly elastic relation is adopted (the weak attenuation being amenable to treatment by perturbation theory) and $\mathbf{T} = \mathbf{C} : \boldsymbol{\epsilon}$ where $\boldsymbol{\epsilon}$ is the strain tensor and $\mathbf{C}$ is a fourth-order tensor of elastic moduli. In component form, the constitutive relation is

$$T_{ij} = C_{ijkl} \epsilon_{kl}$$

where summation over repeated indices is implied. The

most general elastic Earth exhibiting spherical symmetry is "transversely isotropic" (i.e. seismic velocities in the radial direction are different from velocities in the tangent plane) and is described by five elastic moduli which, in Love notation, are: A, C, L, N, and F. An elastically isotropic body is described by two elastic moduli: λ and μ where μ is known as the shear modulus or rigidity. The results for an isotropic body can be recovered from those for a transversely isotropic body using the substitutions: $A = C = \lambda + 2\mu$, $F = \lambda$, and $L = N = \mu$.

Substitution of these forms into equation 8 and 9 results in four coupled second-order ordinary differential equations governing the radial dependence of the scalars in equation 11. (For clarity, we drop the subscripts on U, V, W, and Φ so, in the next equation $U \equiv {}_kU_l^m$ etc.)

$$\frac{1}{r^2}\left(\frac{d}{dr}\ r^2\frac{d\Phi_1}{dr}\right) - l(l+1)\frac{\Phi_1}{r^2} =$$

$$- 4\pi G\left[\frac{d}{dr}(\rho_0 U) + \rho_0 F\right]$$

$$-\rho_0\omega_k^2 U = \frac{d}{dr}\left(CU' + FF\right)$$

$$-\frac{1}{r}\left[2(F - C)U' +2(A - N - F)F + l(l+1)LX\right]$$

$$-\rho_0\Phi_1' + g_0\left((\rho_0 U)' + \rho_0 F\right) - (\rho_0 g_0 U)'$$

$$-\rho_0\omega_k^2 V = \frac{d}{dr}(LX)$$

$$+\frac{1}{r}\left[(A - N)F + FU' + 3LX - \frac{NV}{r}(l+2)(l-1)\right]$$

$$-\frac{\rho_0\Phi_1}{r} - \frac{\rho_0 g_0 U}{r}$$

$$\left.\right\} \tag{13}$$

$$-\rho_0\omega_k^2 W = \frac{d}{dr}(LZ)$$

$$+\frac{1}{r}\left[3LZ - \frac{NW}{r}(l+2)(l-1)\right] \tag{14}$$

where

$$X = V' + \frac{U - V}{r}$$

$$Z = W' - \frac{W}{r}$$

$$F = \frac{1}{r}(2U - l(l+1)V)$$

and a prime denotes radial derivative. Note that the equations are dependent upon harmonic degree (ℓ) but are independent of azimuthal order number m. Consider equation 14. For a chosen harmonic degree and frequency, the solution to these equations will not necessarily match the boundary conditions (notably vanishing of traction at the free surface). There are however, discrete frequencies for each ℓ when solutions $W(r)$ can be found which match all boundary conditions. Such frequencies are the frequencies of free toroidal oscillation of the Earth. For a particular ℓ, the mode with the lowest frequency of free oscillation is labelled ${}_0T_\ell$, the next highest is ${}_1T_\ell$ and so on. The displacement field of the n'th mode ${}_nT_\ell$ which has frequency ${}_n\omega_\ell$ say is proportional to

$$_n\mathbf{s}_l^m = \left[\hat{\boldsymbol{\theta}}\cosec\theta\ {}_nW_l(r)\frac{\partial Y_l^m}{\partial\phi} - \hat{\boldsymbol{\phi}}\ {}_nW_l(r)\frac{\partial Y_l^m}{\partial\theta}\right]e^{i\ {}_n\omega_l t} \tag{15}$$

for $-l \le m \le l$. This kind of motion is called toroidal because it consists of twisting on concentric shells. Toroidal motion can be sustained only in a solid so toroidal modes are confined to the mantle (another class is confined to the inner core but cannot be observed at the surface). Note that there is no radial component of motion and no compression or dilation so there is no perturbation to the gravitational field. This is not true for solutions to the other three coupled ODEs (equation 13). Again there are discrete frequencies for a fixed harmonic degree where solutions can be found which match all boundary conditions. These are the frequencies of free spheroidal motion (sometimes called poloidal motion). For a particular ℓ, the mode with the lowest frequency of free oscillation is labelled ${}_0S_\ell$, the next highest is ${}_1S_\ell$ and so on. The displacement field of the n'th mode ${}_nS_\ell$ which has frequency ${}_n\omega_\ell$ say is proportional to

$$_n\mathbf{s}_l^m = \left[\hat{\mathbf{r}}\ {}_nU_l(r)Y_l^m(\theta,\phi) + \hat{\boldsymbol{\theta}}\ {}_nV_l(r)\frac{\partial Y_l^m}{\partial\theta}(\theta,\phi)\right.$$

$$\left. + \cosec\theta\hat{\boldsymbol{\phi}}\ {}_nV_l(r)\frac{\partial Y_l^m}{\partial\phi}(\theta,\phi)\right]e^{i_n\omega_l t} \tag{16}$$

Note that in both equations 15 and 16, for each n and ℓ there are $2\ell + 1$ modes of oscillation with exactly the same frequency (since the governing equations don't depend upon m). This is the phenomenon of degeneracy which is a consequence of the assumed symmetry of the Earth model. This group of $2\ell + 1$ modes is called a "multiplet" while the individual members of the multiplet are called "singlets". Departures of the Earth from spherical sym-

metry remove the degeneracy and, in general, each singlet within a multiplet will have a slightly different frequency.

We can also use the results given above to compute the elastic energy density of a mode. The total elastic energy of a mode is:

$$E = \int_V \epsilon^* \cdot \mathbf{C} : \epsilon \, dV \qquad (17)$$

where the double dots indicate tensor contraction. This can be written in terms of the mode scalars as:

$$E = \int \left[l(l+1)(l-1)(l+2)\frac{N}{r^2}W^2 + l(l+1)LZ^2 \right] r^2 \, dr \qquad (18)$$

for toroidal modes, and

$$E = \int \left[l(l+1)(l-1)(l+2)\frac{N}{r^2}V^2 + l(l+1)LX^2 \right.$$
$$\left. +2FU'F + (A-N)F^2 + CU'^2 \right] r^2 \, dr \qquad (19)$$

for spheroidal modes. For an elastically isotropic material, we can divide the elastic energy into its shear and com-

pressional components by substituting the bulk modulus K_s for λ using the relationship $K_s = \lambda + 2/3\mu$ yielding

$$E = \int \left[\frac{\mu}{r^2}l(l+1)(l-1)(l+2)W^2 + \mu l(l+1)Z^2 \right] r^2 \, dr \qquad (20)$$

for toroidal modes, and

$$E = \int \left[\frac{\mu}{r^2}l(l+1)(l-1)(l+2)V^2 + \mu l(l+1)X^2 \right.$$
$$\left. +\frac{\mu}{3}(2U'-F)^2 + K_s(U'+F)^2 \right] r^2 \, dr \qquad (21)$$

for spheroidal modes. The integrands are plotted in Figures 5 and 6 for some representative modes of oscillation.

REFERENCES

1. Z. Alterman, H. Jarosch, and C.L. Pekeris, Oscillations of the Earth. *Proc. Roy. Soc.*, **A252**, 80–95, 1959.

2. G.E. Backus, and J.F. Gilbert, The rotational splitting of the free oscillations of the earth. *Proc. Natl. Acad. Sci.*, **47**, 362–371, 1961.

3. H. Benioff, Long waves observed in the Kamchatka earthquake of November 4, 1952. *J. Geophys. Res.*, **63**, 589–593, 1958.

4. R. Buland, J. Berger, and F. Gilbert, Observations from the IDA network of attenuation and splitting during a recent earthquake. *Nature*, **277**, 358–362, 1979.

5. B.F. Chao, and F. Gilbert, Autoregressive estimation of complex eigenfrequencies in low frequency seismic spectra. *Geophys. J. R. Astron. Soc.*, **63**, 641–657, 1980.

6. F.A. Dahlen, The spectra of unresolved split normal mode multiplets. *Geophys. J. R. Astron. Soc.*, **58**, 1–33, 1979.

7. F.A. Dahlen, The free oscillations of an anelastic aspherical earth. *Geophys. J. R. Astron. Soc.*, **66**, 1–22, 1981.

8. J.P. Davis, Local eigenfrequency and its uncertainty inferred from fundamental spheroidal mode frequency shifts. *Geophys. J. R. Astron. Soc.*, **88**, 693–722, 1987.

9. J.S. Derr, Free oscillation observations through 1968. *Bull. Seismol. Soc. Am.*, **59**, 2079–2099, 1969.

10. J.J. Durek, and G. Ekström, Differences between observations of fundamental mode attenuation. *EOS Trans. AGU*, **73**, 402, 1992.

11. A.M. Dziewonski, and D.L. Anderson, Preliminary reference Earth model. *Phys. Earth Planet. Inter.*, **25**, 297–356, 1981.

12. A.M. Dziewonski, and J.F. Gilbert, Observations of normal modes from 84 recordings of the Alaskan earthquake of 28 March 1964. *Geophys. J. R. Astron. Soc.*, **27**, 393–446, 1972.

13. A.M. Dziewonski, and J.F. Gilbert, Observations of normal modes from 84 recordings of the Alaskan earthquake of 28 March 1964 II. *Geophys. J. R. Astron. Soc.*, **35**, 401–437, 1973.

14. D. Giardini, X.-D. Li, and J.H. Woodhouse, Three-dimensional structure of the earth from splitting in free oscillation spectra. *Nature*, **325**, 405–411, 1987.

15. D. Giardini, X.-D. Li, and J.H. Woodhouse, Splitting functions of long period normal modes of the earth. *J. Geophys. Res.*, **93**, 13,716–13,742, 1988.

16. F. Gilbert, and A.M. Dziewonski, An application of normal mode theory to the retrieval of structural parameters and source mechanisms from seismic spectra. *Phil. Trans. R. Soc. Lond.*, **A278**, 187–269, 1975.

17. S. Hori, Y. Fukao, M. Kumazawa, M. Furumoto, and A. Yamamoto, A new method of spectral analysis and its application to the Earth's free oscillations: The "Sompi" method. *J. Geo-*

phys. Res., **94**, 7537–7553, 1989.

18. T.H. Jordan, A procedure for estimating lateral variations from low-frequency eigenspectra data. *Geophys. J. R. Astron. Soc.*, **52**, 441–455, 1978.

19. E.R. Lapwood, and T. Usami, *Free Oscillations of the Earth*. Cambridge University Press, New York, 1981.

20. X.-D. Li, D. Giardini, and J.H. Woodhouse, Large-scale, three-dimensional, even degree structure of the Earth from splitting of long-period normal modes. *J. Geophys. Res.*, **96**, 551–577, 1991.

21. G. Masters, and F. Gilbert, Attenuation in the earth at low frequencies. *Phil. Trans. R. Soc. Lond.*, **A308**, 479–522, 1983.

22. G. Masters, T.H. Jordan, P.G. Silver, and F. Gilbert, Aspherical earth structure from fundamental spheroidal-mode data. *Nature*, **298**, 609–613, 1982.

23. G. Masters, J. Park, and F. Gilbert, Observations of coupled spheroidal and toroidal modes. *J. Geophys. Res.*, **88**, 10,285–10,298, 1983.

24. J. Park, C.R. Lindberg, and D. Thomson, Multiple-taper spectral analysis of terrestrial free oscillations: Part I. *Geophys. J. R. Astron. Soc.*, **91**, 755–794, 1987.

25. C.L. Pekeris, Z. Alterman, and H. Jarosch, Rotational multiplets in the spectrum of the earth. *Phys. Rev.*, **122**, 1692–1700, 1961.

26. M. Ritzwoller, G. Masters, and F. Gilbert, Observations of anomalous splitting and their interpretation in terms of aspherical structure. *J. Geophys. Res.*, **91**, 10,203–10,228, 1986.

27. M. Ritzwoller, G. Masters, and F. Gilbert, Constraining aspherical structure with low frequency interaction coefficients: Application to uncoupled multiplets. *J. Geophys. Res.*, **93**, 6369–6396, 1988.

28. B. Romanowicz, G. Roult, and T. Kohl, The upper mantle degree two pattern: constraints from GEOSCOPE fundamental spheroidal mode eigenfrequency and attenuation measurements. *Geophys. Res. Lett.*, **14**, 1219–1222, 1987.

29. G. Roult, and B. Romanowicz, Very long-period data from the geoscope network: Preliminary results on great circle averages of fundamental and higher Rayleigh and Love modes. *Bull. Seismol. Soc. Am.*, **74**, 2221–2243, 1984.

30. G. Roult, B. Romanowicz, and J.P. Montagner, 3-D upper mantle shear velocity and attenuation from fundamental mode free oscillation data. *Geophys. J. Int.*, **101**, 61–80, 1990.

31. P.G. Silver, and T.H. Jordan, Fundamental spheroidal mode observations of aspherical heterogeneity. *Geophys. J. R. Astron. Soc.*, **64**, 605–634, 1981.

32. M.F. Smith, Imaging the Earth's aspherical structure with free oscillation frequency and attenuation measurements. Ph.D Thesis, Univ. Cal. San Diego, La Jolla, CA, 1989.

33. M.F. Smith, and G. Masters, Aspherical structure constraints from free oscillation frequency and attenuation measurements. *J. Geophys. Res.*, **94**, 1953–1976, 1989.

34. R. Widmer, *The large-scale structure of the deep Earth as constrained by free oscillation observations*. Ph.D. Thesis Univ. Cal. San Diego., 1991.

35. R. Widmer, G. Masters, and F. Gilbert, Spherically symmetric attenuation within the Earth from normal mode data. *Geophys. J. Int.*, **104**, 541–553, 1991.

36. R. Widmer, G. Masters, and F. Gilbert, Observably split multiplets – data analysis and interpretation in terms of large-scale aspherical structure. *Geophys. J. Int.*, **111**, 559–576, 1992.

37. Widmer, R. W. Zürn, and G. Masters, Observations of low order toroidal modes from the 1989 Macquarie Rise event. *Geophys. J. Int.*, **111**, 226–236, 1992.

38. Y.K. Wong, *Upper mantle heterogeneity from phase and amplitude data of mantle waves*. Ph.D Thesis, Harvard University, Cambridge, 1989.

39. J.H. Woodhouse, and F.A. Dahlen, The effect of a general aspherical perturbation on the free oscillations of the earth. *Geophys. J. R. Astron. Soc.*, **53**, 335–354, 1978.